Energy Aware Network Optimization with Aerial Base Stations

Jingcong Sun

A thesis submitted for the degree of

Master of Philosophy

of

University College London.

Department of Electronic and Electrical Engineering

University College London

May 28, 2019

I, Jingcong Sun, confirm that the work presented in this thesis is my own. Where information has been derived from other sources, I confirm that this has been indicated in the thesis.

Sign:

Date:

Abstract

To meet the fast-growing and highly diversified traffic demand, it is envisioned that unmanned aerial vehicles (UAVs), also known as drones, will become an indispensable part in the future communication system. Since UAVs are flexible, cost-effective, fast to deploy and have a better communication condition compared to terrestrial communication system, the use of drones is promising in a wide range of wireless networking applications. By moving closer to the targets, UAVs can act as data collectors to prolong the lifetime of wireless sensor networks (WSNs) or be used as energy transmitters to transfer more energy in wireless power transfer (WPT) scenarios. In particular, UAV based aerial base stations (BSs) have the ability to provide rapid and reliable wireless services wherever and whenever there is an excessive data demand and has become increasingly appealing to network service providers.

In this thesis, we focus on UAVs serving as BSs to provide wireless services to ground users from the sky. Firstly, we consider the power-efficient deployment of multiple static aerial BSs, with the aim of covering a maximum number of ground users while avoiding inter-cell interference (ICI). The proposed techniques achieve an up to 30% higher coverage probability then the benchmark circle packing theory (CPT) when users are not distributed uniformly. In addition, the proposed iterative algorithm also greatly improves the power-efficiency by up to 15%. Secondly, by fully exploiting the mobility of UAVs, we study the trajectory and UAV-user scheduling and association of moving aerial BSs. The bottom line aim of UAV application, where an aerial BS is dispatched to satisfy the data demand of a maximum number of ground users with a given energy budget is considered. It is found that

the moving aerial BS tends to move close to the targeted ground users to reduce path loss and enjoy a good communication condition. Simulation results show both energy and coverage performance gains for the proposed schemes compared to the benchmark techniques

Impact Statement

The research in this thesis has contributed to the energy-efficient deployment and trajectory design of UAV based aerial BS, which is an indispensable part in future communication systems. From the perspective of academia, this research has studied the bottom line aim of aerial BSs, trying to cover a maximum number of ground users with minimum energy. This research relates to the aims of the MSCA-ITN-ETN project PAINLESS that UCL is coordinating. In fact, this research topic has also attracted the attention of many world-leading companies. Facebook, Nokia-bell labs, China Mobile and Google have successively launched pilot projects to provide wireless services with aerial BSs. In addition, both Qualcomm and AT&T have optimized LTE networks, targeted for possible wide-scale UAV-communications, especially for mission-critical use cases.

Notably, the research in this thesis is relevant in public safety scenarios. Terrestrial communication infrastructures can be damaged or completely destroyed during natural disasters and other unexpected events. The recent aftermath of Hurricanes Sandy is a strong evidence. In such scenarios, aerial BSs which are flexible and able to provide fast service recovery play a vital role in public safety communication between victims and first responders for search and rescue. Therefore, the work in this thesis not only contribute to improving wireless connectivity, but also to saving lives in public safety scenarios.

Acknowledgements

First of all, I would like to thank my parents for supporting me to pursue my MPhil abroad. Thanks for backing me up and support every decision I made.

I would like to give my greatest gratitude to my supervisor, Dr. Christos Masouros for offering me this great opportunity to study in UCL. I am deeply encouraged by his enthusiasm towards research and it is his valuable guidance and detailed advice that have motivated me to accomplish all these.

I would like to express my special thanks to Miss. Zhuoyun Yao for the understanding, encouragement, and all the joy and sorrow we share together.

Last but not the least, I would like to thank Dr. Fan Liu, Dr Ang Li, Dr Lifeng Wang and Dr. Zhongxiang Wei for sharing their rich knowledge and experience. I would like to be thankful to all my colleagues.

Contents

List of Abbreviations

5G	Fifth Generation
D2D	Device-to-device
M-MIMO	Massive MIMO
mmWave	Millimeter Wave
BS	Base Station
UAV	Unmanned Aerial Vehicle
LoS	Line of Sight
ICI	Inter-cell Interference
ULI	User Location Information
MILP	Mixed Integer Linear Problem
MINLP	Mixed Integer Non-linear Problem
HAP	High-altitude Platform
LAP	Low-altitude Platform
AtG	Air-to-ground
WPT	Wireless Power Transfer
IoT	Internet of Things
QoS	Quality of Service
CMA	Cyclical Multiple Access

CTDMA	Cyclical Time Division Multiple Access
NLoS	Non-line of Sight
FSPL	Free Space Path Loss
SNR	Signal-to-noise Ratio
SINR	Signal-to-interference-plus-noise Ratio
FDMA	Frequency Division Multiple Access
TDMA	Time Division Multiple Access
CDMA	Code Division Multiple Access
SDMA	Space Division Multiple Access
SS	Spread Spectrum
PN	Pseudo-noise
SPP	Spatial Point Process
HPP	Homogeneous Poisson Process
IPP	Inhomogeneous Poisson Process
PCP	Poisson Cluster Process
CPT	Circle Packing Theory
CDF	Cumulative Distribution Function
GPS	Global Positioning System
SDR	Semidefinite Relaxation
SD-GR	Successive Deployment Method with Geometrical Relaxation
SD-KM	Simultaneous Deployment Method with K-means Clustering

SD-KMVR	Simultaneous Deployment Method with Variable Radius
LHS	Left-hand-side
CIT	Circular Initial Trajectory
DIT	Designed Initial Trajectory

List of Notations

a	Scalar
$\mathbf{a}$	Vector
$\mathbf{A}$	Matrix
$\mathrm{P_r}(.)$	Probability
$\mathrm{E}\{.\}$	Expectation of a random variable
$\lceil . \rceil$	Ceiling function
$\tan(.)$	Tangent function
$\mathscr{O}$	Computational complexity
$\lvert . \rvert$	Cardinality
$(.)^T$	Transpose of a vector/matrix
$\lvert\lvert . \rvert\rvert$	Frobenius Norm

List of Figures

List of Tables

Chapter 1

Introduction

1.1 Background and Literature Review

1.1.1 Potential Use Cases of UAV-enabled wireless networks

To satisfy the incessantly increasing and highly diversified data demand for the upcoming fifth-generation (5G) mobile communication system, researchers have devoted significant efforts to exploring new wireless technologies, such as massive multiple-input multiple-output (M-MIMO), millimeter wave (mmWave) and device-to-device (D2D) communication [1–4]. Despite the significant benefits, all these technologies were mainly designed for terrestrial communication systems with fixed ground base stations (BSs) and have their own drawbacks and limitations.

Recently, there have been increased interests in providing wireless communication services from the sky. One solution is using high-altitude platforms (HAPs), such as airships and balloons [5, 6]. Since HAPs are usually operate at a high altitude which is tens of kilometers above the ground, such platforms can offer wide coverage area and usually have long endurance [7]. On the other hand, unmanned aerial vehicle (UAV) based low-altitude platforms (LAPs) have several advantages compared to the terrestrial communication and HAP based communication. For instance, UAVs are more swift, flexible and cost-effective [8]. In addition, drones are usually deployed at an altitude of several hundred meters, so there is a large probability of short-range line-of-sight (LoS) air-to-ground (AtG) communication

channel. Undoubtedly, thanks to the advantages mentioned above, UAVs are regarded as an inevitable complement in future communication systems, which will bring unique benefits of its own and enable to address some problems of existing technologies.

It is known that D2D networks enable direct communication between mobile devices without going through BSs, and thus improve the performance regarding spectral efficiency and access delay [9, 10]. However, reliable and efficient communication performance can only be achieved within short communication range and direct communication among various access points may cause severe interference issues. Use of UAV is a potential way to overcome the challenges in D2D networks [11–13]. The main advantage of UAV-assisted D2D networks is that the use of UAVs greatly reduces the number of required transmission links among ground devices, thus mitigates the interference in the D2D networks. Besides, due to the flexibility and maneuverability, UAVs can disseminate emergency information to a large number of devices, which is relevant in public safety situations [11].

Catering for reliable communication and high data rate, the 5G cellular paradigm tries to exploit the underutilized millimeter-wave (mmWave) spectrum [2, 14, 15]. However, the mmWave links also lead to high path loss and are susceptible to obstacles along the communication path. UAVs which fly in the air and enjoy LoS AtG communication condition is an ideal enabler for mmWave communication [15–18]. On one hand, with UAVs as enablers, the communication link can be hardly blocked and the path loss is greatly reduced. On the other hand, equipped with multiple small size antennas, UAVs can realize the more advanced massive MIMO techniques from the sky.

In addition, use of UAVs is promising in the Internet of Things (IoT) networks which have a strict requirement on energy efficiency and reliability. In general, IoT devices are highly battery-limited and have a short communication range [19–22]. In addition, since IoT devices have various applications, they might be deployed in places where there is a poor coverage or even no coverage of terrestrial cellular networks [13, 22]. The above challenges can be efficiently solved with UAVs serving

as aerial base stations (BSs). First, due to the flexibility of UAV, aerial BSs can be deployed based on the location of IoT devices and the devices are only associated with UAV when there is a good enough communication condition. In this way, the IoT devices can transmit information with a clearly reduced transmit power and the life time of the IoT network is greatly increased correspondingly [19, 20, 22–24]. Second, aerial BSs can be deployed in areas with no ground communication infrastructures such as mountains to enable the function of IoT devices.

In fact, UAV based aerial BSs can provide fast and reliable wireless services wherever and whenever there is an excessive data requirement and is another main application of UAV. While ultra dense small cell networks are envisioned as an important part in 5G communication system to further improve the throughput, deploying such networks is challenging in geographically constrained areas [25]. Meanwhile, terrestrial communication infrastructures can be severely damaged or even completely destroyed during natural disasters such as hurricane and earthquake. Aerial BSs, on the other hand, can fly to any places and are able to provide fast service recovery in emergency or disaster scenarios [11, 26, 27]. Moreover, aerial BSs can also ease the burden of terrestrial base stations in extremely crowded areas by offloading a part of users from ground cells [28]. This is especially useful in the cases of temporary events such as Olympic games where it is not cost effective to deploy multiple small ground cells.

Another promising use of UAV is relaying [29, 30]. Currently, most relays are deployed in fixed locations due to constraints like wired backhaul and limited mobility. This limits the use of relay in more specific scenarios such as battlefield. When UAV is used for mobile relaying, it extends the coverage and increases the throughput from the source node to the destination node by dynamically flying closer to the node which has a communication demand [23, 31–34].

Besides all the use cases mentioned above, wireless power transfer (WPT) is also an application which benefits from the mobility of the UAV. In conventional WPT systems, energy transmitters are deployed at fixed locations to charge the energy receivers. Therefore, for addressing the low power transmission efficiency

Table 1.1: Potential UAV-enabled communication applications

Use Cases	Drawback of Existing Technology	Main Advantage of using UAV	Key References
D2D networks	• Interference among mobile devices • short communication range	• Mitigate interference issue • Improve connectivity • Broadcast emergency information	[11–13, 35]
Enabler for mmWave	• Bad performance in multi-path fading environment • High path loss	• Bring LoS communication condition	[15–18, 36]
IoT networks	• Battery-limited IoT devices • Short communication distance • Bad performance in geographically constrained areas	• Improve endurance of IoT networks • improve communication condition • Enable IoT devices in geographically constrained areas	[19, 20, 22–24]
Aerial BSs	• Expensive terrestrial infrastructures • Susceptible to natural disasters	• Cost effective • Service recovery in emergency or disaster scenarios • Ease the burden of ground cells	[11, 26–28, 37, 38]
Relaying	• Fixed locations and limited performance	• Improve communication performance • Wide application scenario	[23, 31–34]
WPT	• Low power transmission efficiency • Expensive infrastructures	• Increase transmission efficiency with lower cost	[39, 40]

due to the long communication distance, the energy transmitters need to be placed in an extremely dense manner which increases the cost [39]. UAV-enabled WPT can greatly increase the energy transferred to all energy receivers by flying close to the targets and reduce the energy loss [40].

For brevity, we summarize all the potential use cases of UAV in Table 1.1. Note that, in this paper, we restrict our attention to UAV-aided aerial BSs, which might be the most imminent application. In the following section, we review the

state-of-the-art and show the main research directions as well as the challenges regarding deploying aerial BSs.

1.1.2 Research Direction and Challenges of aerial BSs

With the rising interest in deploying aerial BSs to achieve better communication performance, the challenges in the practical use of aerial BSs are becoming pertinent.

1.1.2.1 AtG Channel Modeling

The first research topic that plays an important role in the real application of aerial BSs is the accurate modelling of AtG communication channel. Although AtG communication links are dominated by LoS links in general, they can be occasionally blocked by obstacles such as buildings and terrains [11]. The probability of NLoS links becomes non-negligible in highrise urban environments [26]. While ray-tracing technique is widely utilized for approximating the AtG channels, it still lacks accuracy [41].

Recently, the AtG modelling problem has been extensively studied in the literature. For example, authors in [42] gave an model of AtG channel while considering the possible effects of small-scale fadings. The work [43] verified that AtG links experience less shadowing and path loss than the channels in terrestrial communication systems. An elevation dependent shadowing model is then presented in [44]. It is worth highlighting that [26] gives a simplified model of AtG channel by considering the probability of both LoS and NLoS links.

1.1.2.2 Deployment of Static Aerial BSs

Since aerial BSs can hold stationary in the air, providing coverage to ground users, the priority of static aerial BSs is finding the optimal locations of UAVs so that a maximum number of ground users can be covered. This is relevant in emergency scenarios such as search-and-rescue after natural disasters and rural area scenarios where there is no ground infrastructures. The optimal three dimensional placement

of UAVs is challenging as it is affected by a large number of factors such as UAV's altitude, AtG channel characteristics, locations of ground users and specific deployment environment. When more than one aerial BS is deployed, the effect of ICI should also be considered, which further challenges the successful deployment of UAVs [45, 46].

The aerial BS coverage problem was first studied in [26], which gave an AtG channel model used to find the optimal altitude of UAVs that can lead to maximum coverage area on the ground. Moreover, recent research focus has shifted from maximizing the coverage area towards covering a maximum number of ground users [27, 28, 37, 47]. Specifically, [47] formulated a 3-D circle placement problem as a MINLP and solved the problem with convex optimization techniques. In [28], the authors did an exhaustive search in girds to obtain the optimal location of an aerial BS. However, all the works mentioned above considered only the case of a single static aerial BS which limits their use. Unlike HAPs such as balloon and airships, UAV which is a typical LAP has a limited coverage area of around several square kilometers. In practice, it is usually a necessity to deploy multiple UAVs simultaneously so a majority of ground users in a specific target region can be covered. Mozaffari*et al.* [45] first extended the number of used aerial BSs to two with a careful consideration of ICI. Then the same group [48] proposed a circle packing theory (CPT) so that the total coverage area of multiple aerial BSs is maximized. However, the work did not consider the effect of different user distributions. In [49], a 100% user coverage probability is achieved through a spiral algorithm, however, the study ignores the effect of ICI which needs to be tackled with overlaid techniques.

1.1.2.3 Trajectory Design of Moving Aerial BSs

The potential of aerial BSs can be fully exploited by leveraging the mobility of UAVs. Correspondingly, trajectory design of UAVs might be the main challenge involved in UAV-based aerial BSs. In general, the trajectory design of UAV requires jointly considering the constraints with regard to flying status, flight time, collision

avoidance, scheduling and user demand [11]. Moreover, for solving a continuous UAV trajectory optimization problem, one needs to tackle with an infinite number of optimization variables. All these factors make the trajectory design of aerial BSs challenging.

Significant efforts have been devoted to solving the trajectory optimization problem [20,50–53]. By assuming the users are distributed along a one-dimensional line, a novel cyclical multiple access (CMA) method was proposed for moving aerial BSs in [51]. Authors in [20] jointly optimize the UAV trajectory and user scheduling variables to increase the maximum throughput gain. In addition, the works in [54] studied the path planning for localization purposes. [53] offloads the data traffic of cell edge users by letting a moving aerial BS fly cyclically around a ground BS. In [55], the optimal trajectory of a UAV deployed with multiple antennas was investigated for the aim of sum-rate maximization.

1.1.2.4 Energy Efficiency

Last but not the least, since UAVs use built-in batteries for supplying power in most cases, limited on-board energy is a key factor that constrains the performance and endurance of aerial BSs [11, 56–58]. Both communication functions and moving properties consume the built-in energy. In general, the expression of the propulsion power which is a function of the flying status of UAV is hard to be derived and is normally non-convex.

For static aerial BSs where the UAVs remain stationary in the sky, it has been proven that prolonged operation time can be achieved by reducing the transmit power as long as the quality-of-service (QoS) requirements are satisfied [47, 59]. For moving aerial BSs, however, the consumed propulsion energy is much larger than the communication-related energy. Therefore, trajectory design takes an important part in energy efficient communication when mobility of the UAV is exploited. Without considering the propulsion energy for supporting the movement of UAVs, efficient usage of energy for communication related functions have been studied in [60–62]. Authors in [24] took the propulsion power consumption into

Table 1.2: Research directions and challenges

Research Directions	Challenges	Representative Techniques	Key References
AtG channel modeling	• Various environment • Path loss • Small-scale fadings	• Extensive measurements • Ray Tracing technqiues	[26, 42–44]
Deployment of static aerial BSs	• 3-D deployment • ICI • Energy efficient deployment	• Circle packing Theory (CPT) • Machine Learning algorithms • Spiral Algorithm	[26–28, 37, 47–49]
Trajectory design of moving aerial BSs	• Massive coupled constraints • Energy-aware trajectory • Infinite number of optimization variables	• Convex optimization • Machine learning algorithms • Discretization methods	[20, 50–53, 55]
Energy efficiency	• Power consumption model • Energy-performance Tradeoff	• Convex optimization • Machine learning algorithms	[24, 47, 59–63]

consideration and gave a model of consumed propulsion power of fixed wing UAVs. Moreover, authors in [63] minimize the total power consumption of a UAV with a guaranteed transmission rate.

For simplicity, we summarise the main research directions as well as the challenges in these areas in Table 1.2. In this thesis, we focus on the coverage performance and endurance of aerial BSs. Both the optimal deployment of static aerial BSs and the optimal trajectory of moving aerial BSs are studied. To be specific, when multiple static aerial BSs are deployed, we try to maximize the number of covered ground users while avoiding the effect of inter-cell interference (ICI). In addition, when moving aerial BS is considered, we try to satisfy the data demand of a maximum number of ground users by optimizing the trajectory and UAV-user scheduling with a given energy budget, which is the bottom line aim of UAV application. The detailed contributions can be found in the following section.

1.2 Contributions

In this thesis, we study the coverage performance of both static aerial BS and moving aerial BS. Regarding static aerial BS, we consider a scenario that multiple aerial BSs are deployed simultaneously to cover a maximum number of ground users while avoiding ICI. Therefore, it is of great interest to study the optimal location of aerial BSs. Since the endurance of aerial BSs is limited by the on-board energy, we minimize the transmission power to prolong the battery life of UAVs. Regarding moving aerial BS, we consider a scenario that an aerial BS is dispatched to meet the data demand of a maximum number of ground users before exhausting its limited on-board energy and flying back to the base for charging. It is mentionable that perfect user location information (ULI) may not available in practice, so we propose various robust techniques for compensating the performance loss in the existence of inaccurate ULI. The main contributions of this thesis are summarized as follows:

- UAV Positioning Optimization (Chapter 3): With regard to the static aerial BS scenario, we first propose a successive deployment scheme, in which the next aerial BS is always deployed in a position such that a maximum number of remaining users in the target area can be covered. The resulting optimization problem involves a increased number of non-convex constraints which are tackled with a simple geometrical relaxation method. After that, a more efficient technique which deploys all the aerial BSs simultaneously is proposed with the help of K-means clustering. In the simultaneous deployment method, the whole target area is divided into multiple polygon regions where convex optimization problems can be solved. Furthermore, an iterative algorithm is further proposed to improve the coverage performance while reducing the required transmit power consumption. Finally, a robust technique is proposed to maximize the number of covered users in the existence of imperfect ULI and the computational complexity of all the proposed techniques are derived analytically.

- UAV Trajectory Optimization (Chapter 4): By fully exploiting the mobility of UAV, we try to satisfy the data requirement of a maximum number

of ground users while considering constraints on energy resources. The formulated mixed integer non-linear problem (MINLP) is solved by an efficient iterative algorithm where successive convex optimization and block coordinate descent techniques are applied. Next, since the convergence speed and achievable performance of such iterative algorithm depends on the adopted initial trajectory, we design an initial trajectory which gives all users a relatively fair chance to be scheduled and associated. In addition, the existence of inaccurate ULI is also considered, and we propose two different robust techniques to compensate the loss in coverage performance. Specifically, the first robust technique optimizes the worst case coverage performance and the second robust technique maximizes the minimum excess data for the covered ground users.

Based on the above contributions, we have produced academic papers for publication which are listed below.

1.3 List of Publications

1.3.1 Accepted Papers

1. J. Sun and C. Masouros, "Deployment Strategies of Multiple Aerial BSs for User Coverage and Power Efficiency Maximization," *IEEE Transactions on Communications*, Early Access, URL: https://ieeexplore.ieee.org/document/8587183

2. J. Sun and C. Masouros, "Drone Positioning for User Coverage Maximization," *2018 IEEE 29th Annual International Symposium on Personal, Indoor and Mobile Radio Communications (PIMRC)*, Bologna, 2018, pp. 318-322.

1.3.2 Papers Under Review

1. J. Sun and C. Masouros, "Energy Aware Trajectory Optimization for Aerial Base Stations," *IEEE Transactions on Communications*, under review, submitted 21/01/2019.

1.4 Thesis Organization

The rest of the thesis is organized as follows. In Chapter 2, we introduce the AtG channel model and the fundamental knowledge of multiple access techniques, followed by the description of spatial point process methods which are used to model the user distribution. In Chapter 3, we study the coverage performance of multiple static aerial BSs. After introducing the system model, we first propose one successive deployment technique and two simultaneous deployment techniques to optimize the location of aerial BSs to cover a maximum number of ground users while avoiding the effect of ICI. A robust technique designed for inaccurate ULI and the computational complexity analysis are shown afterwards. In Chapter 4, we first propose an iterative algorithm which optimizes both the trajectory and UAV-user scheduling to meet the data demand of a maximum number of ground users before exhausting the UAV's on-board energy. Next, we show a designed initial trajectory which speeds up the convergence and improves the coverage performance. Two different robust techniques which compensate the performance loss in the existence of imperfect ULI are then studied in this chapter. Finally, in Chapter 5, we conclude the whole thesis.

Chapter 2

Air to Ground (AtG) communication system

2.1 Introduction

In this chapter, we introduce fundamental concepts which are highly related to the AtG communication. We begin with an overview of communication path loss model and indicate the main channel characteristics of AtG communication system. The commonly used performance metrics are also introduced. Next, the main types of multiple access techniques are described followed with the introduction of a new multiple access technique called cyclical time-division multiple access (CTDMA) which is tailored for moving aerial BSs. Since we aim at covering a maximum number of ground users and user distribution exerts a significant effect on the coverage performance, we finally introduce the techniques that are used for modeling the user distribution.

2.2 Path Loss Model

The wireless channel places fundamental limitations on the performance of AtG communication system. Same as terrestrial communication system, the performance of AtG communication is limited by the variations in signal strength due to fading effects. Generally, the fading effects can be classified into two main types, which are large-scale fading effect and small-scale fading effect [64]. The large-scale fading characterizes the mean received signal strength and tells us how much

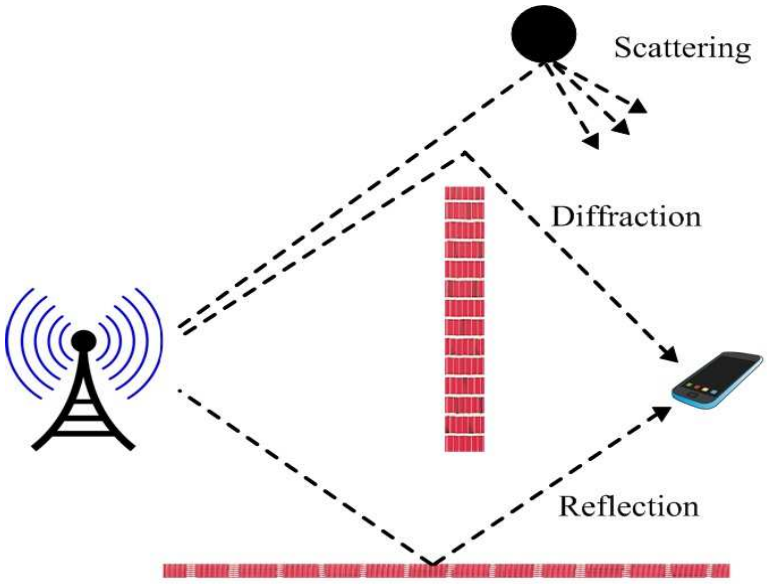

Figure 2.1: An example of reflection, diffraction and scattering components

a signal is going to attenuate over the channel. Small-scale fading effect, on the other hand, characterizes the rapid fluctuations in received signal strength and is a result of multi-path fading.

As depicted in Fig. 2.1, reflection, diffraction and scattering are the main contributors of multi-path fading effect. The received signal through multi-path channel is thus an addition of multi-path components of the transmitted signal and these components can be either constructive or destructive [65]. When different copies of the transmitted signal add destructively, the signal level declines which increases the detection difficulty. Since there are obstacles between the transmitter and the receiver, and the signal is not propagated along a straight line, the paths shown in Fig. 2.1 are all non-line of sight (NLoS) paths. In AtG communication system, however, there is a large probability that there is no obstruction between the transmitter and the receiver, and the communication channel is dominated by short-length LoS path [66]. In the case of LoS link, we have negligible small-scale fadings and the channel quality depends only on the distance between the transmitter and receiver, which follows free-space path loss (FSPL) model given by

$$\mathrm{PL} = 20\log\left(\frac{4\pi f_c d}{c}\right) \tag{2.1}$$

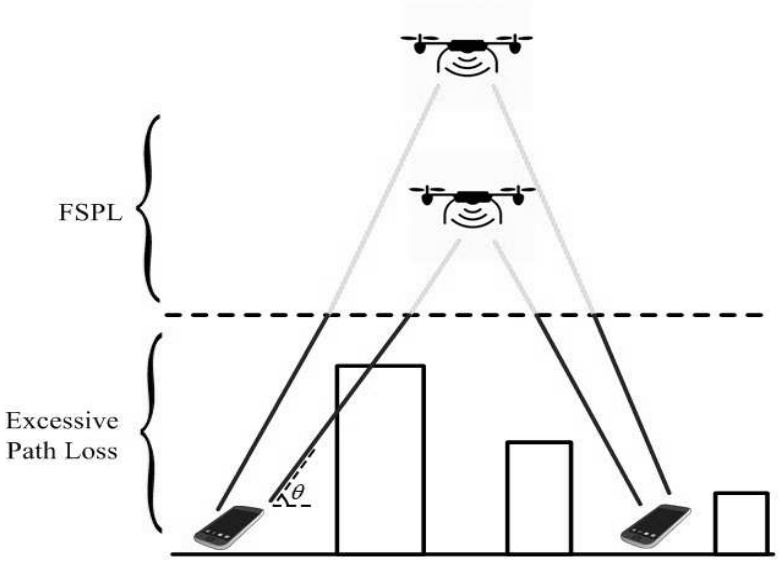

Figure 2.2: An example of AtG channel

where f_c denotes the carrier frequency and d denotes the distance between transmitter and receiver. Although LoS links are expected for AtG communication channels, the channel can be occasionally blocked by obstacles such as buildings in practice [11]. Therefore, following [26], we can describe the probability of LoS link as

$$\mathrm{P_r}(\mathrm{LoS}) = \frac{1}{1 + a\exp(-b[\theta - a])} \tag{2.2}$$

where a and b are parameters related to the specific environment and θ denotes the elevation angle as shown in Fig. 2.2. In dense urban where there is a high density of buildings with high altitude, we have large a and b parameters and thus a small probability of LoS links. In suburban areas, however, buildings are placed sparsely and the communication link can hardly be blocked. In addition, the probability of LoS can be increased by deploying UAVs in a higher altitude. Since $\theta = \arctan(\frac{H}{R})$, with H denotes the altitude of the UAV and R denotes the coverage radius, the elevation angle hence the probability of LoS link can be increased by increasing the altitude of UAV with a fixed radius. This is also verified in Fig. 2.2.

When the AtG channel is blocked by obstacles, the communication suffers additional excessive path loss which is a result of multi-path fading effects. The

NLoS communication channel is thus expressed as

$$\mathrm{PL}_{\mathrm{NLoS}} = 20\log\left(\frac{4\pi f_c d}{c}\right) + \eta_{\mathrm{NLoS}} \tag{2.3}$$

where η_{NLoS} denotes the excessive path loss. For simplicity, we assume that the AtG communication channel is dominated by the LoS links in this thesis.

2.3 Performance Metrics

In this section, performance metrics that are commonly used to evaluate the performance of aerial BS is introduced. We start with the concept of received power and signal-to-noise ratio (SNR) which are two metrics used for determining the coverage area of static aerial BS. Then definition of achievable data bits and coverage probability is given.

2.3.1 Static Aerial BS

When a static aerial BS is deployed, we usually want to maximize the coverage area which is defined as the expected percentage of locations where the received power at these locations is above a certain threshold [65]. All covered ground users require some minimum SNR for maintaining an acceptable communication performance, where SNR is defined as the ratio of received power to the noise power as follows.

$$\mathrm{SNR} = \frac{P_r}{\sigma^2} \tag{2.4}$$

where σ^2 denotes the noise power. Assuming we have a fixed level of noise, the SNR requirement translates to the received power requirement. In other word, all covered users should have a received power larger than a given minimum $P_{\min}$. If we denote the transmit power of aerial BS as P_t and denote the antenna gain as G, the received power in dB is given by

$$P_r = P_t + G - \mathrm{PL} \tag{2.5}$$

Since AtG communication channel is dominated by LoS links as mentioned in the above section, we ignore small-scale fluctuations and the received power threshold $P_{\min}$ indicates a circular coverage area of the aerial BS.

In some specific areas, the signals are frequently blocked and we must consider the shadowing effects. In this case, some locations within the coverage area have received power below $P_{\min}$ and it is impossible for all users located at the coverage boundary to receive same power level [65]. We assume the excessive path loss follows $\eta_{\text{NLoS}} \sim N(\mu_{\text{NLoS}}, \sigma^2_{\text{NLoS}})$, where μ_{NLoS} and σ^2_{NLoS} denote the mean and variance of shadow fading respectively. Therefore, for a ground user which located at a distance $r \leq \frac{H}{\tan\theta}$ from the position of UAV in the horizontal dimension, its coverage probability is given by [48]

$$P_{\text{cov}} = Q\left(\frac{P_{\min} + \text{PL} - P_t - G + \mu_{\text{NLoS}}}{\sigma_{\text{NLoS}}}\right) \tag{2.6}$$

where $Q(.)$ is Q-function described as

$$Q(z) = \int_z^{\infty} \frac{1}{\sqrt{2\pi}} e^{-\frac{x^2}{2}} dx \tag{2.7}$$

Correspondingly, the outage probability is defined as $P_{out} = 1 - P_{\text{cov}}$.

In this thesis, the most important performance metric is coverage probability. When static aerial BS is deployed, coverage probability is defined as the ratio of number of covered ground users to the total number of ground users in a specific target area.

2.3.2 Moving Aerial BS

When the mobility of UAV is exploited, the aerial BS usually associates the ground users in a cyclical time-division manner and an important performance metric is the achievable data of the ground users. We assume the aerial BS uses a total of N time slots to communicate with the ground users, and we define a binary variable $\alpha[n]$ indicating the scheduling and association status of a ground user in time slot n, where $n = 1, 2, ..., N$. To be specific, $\alpha[n] = 1$ indicates that the user is allocated for communicating with the aerial BS at time slot n, $\alpha[n] = 0$ otherwise. If we denote

the SNR in time slot n as $\gamma[n]$, the total achievable data is

$$R = \sum_{n=1}^{N} \alpha[n] B \log_2(1+\gamma[n]) \tag{2.8}$$

where B is the total available bandwidth. Sometimes we focus on the achievable average data rate, which can be obtained by averaging the total achievable data over the whole time period and is thus $\overline{R} = \frac{1}{N}R$.

When moving aerial BS is deployed, we have a different definition for the covered users and thus a different concept of coverage probability. In this case, a user is covered only when his data demand is fully satisfied. Correspondingly, the coverage probability is defined as the ratio of number of satisfied users to the total number of ground users.

2.4 Multiple Access Techniques

In this section, we introduce the multiple access techniques which are commonly used for UAV-enabled communication systems. We start from frequency division multiple access (FDMA) and time division multiple access (TDMA) which are conceptually easy to understand. Then we introduce a new TDMA technique called cyclical time division multiple access (CTDMA) that is designed specifically for moving aerial BSs. In addition, more advanced multiple access techniques such as code division multiple access (CDMA) and space division multiple access (SDMA) are also introduced.

2.4.1 FDMA

Although FDMA might be the oldest multiple access technique which has been used since advanced mobile phone system (AMPS), it still has its usage today and may take an important part in UAV-enabled communication systems. When static aerial BS is deployed, FDMA is the most commonly used multiple access technique in the literature. The core idea of FDMA is that each user is allocated a separate frequency band for transmission during the whole time period. It requires little digital signal processing and has simple temporal synchronization [67]. Unfortunately, FDMA

wastes spectrum and frequency resources

2.4.2 TDMA

In TDMA, a time unit is divided into multiple time slots of fixed length, and each user is assigned one of such time slots [67]. Unlike FDMA, during each time slot, the whole bandwidth is reserved for exclusive use so the user can transmit with higher data rate. Note that TDMA is widely used for moving aerial BSs where the aerial BS only allocates time slots to a ground user when it flies sufficiently close to the user and enjoys the good communication condition. In some scenarios, the UAV is dispatched periodically to serve the ground users, and within each period the ground users are scheduled and associated with TDMA. Such multiple access technique which periodically serves the ground user is also known as CTDMA as proposed in [51].

2.4.3 CDMA

Compared to FDMA and TDMA, CDMA is a more advanced multiple access technique and could be used by aerial BSs. CDMA uses the technology of spread spectrum (SS), where the transmitted spectrum is spread by multiplying the signal with chip sequence [67]. Since the generated chip sequence appears as random noise, the sequence is also known as pseudo-noise (PN) sequence. In CDMA, a unique PN sequence is assigned to each user and the cross-correlation of any two codes are zero, so there is no interference between users [67]. In this case, all active users transmit information simultaneously over the same bandwidth without interfering with each other. At the receiver, correct information can be extracted only when the same PN sequence as used in the transmitter is applied.

2.4.4 SDMA

Due to limited payload and size of UAV, the aerial BSs are usually deployed with single antenna. It is envisioned that multiple antennas may be deployed in aerial BSs to increase the throughput. SDMA is a multiple access technique for systems with multiple antennas. In this method, multiple users can be served simultaneously with the same frequency, because the BS distinguishes different users by means of

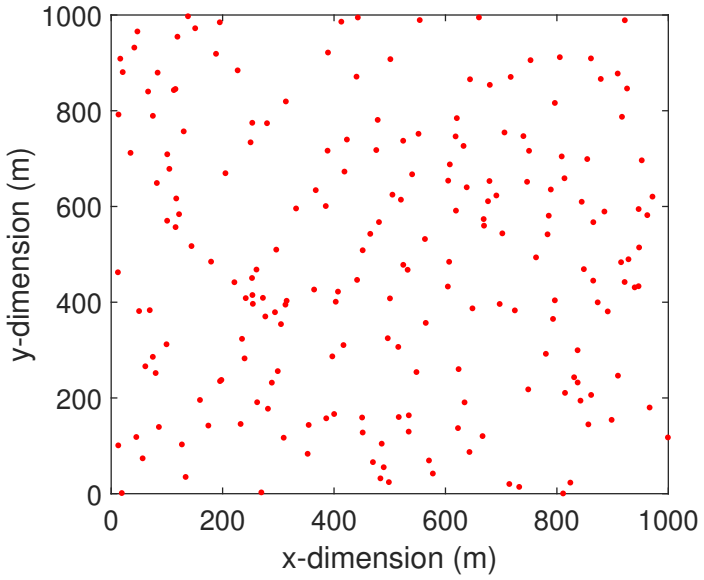

Figure 2.3: An example of user points following HPP with $\lambda_s = 200$

various spatial characteristics. [67].

2.5 User Distribution

In this paper, aerial BSs are deployed to cover a maximum number of ground users. In order to capture a random pattern of ground users in the target area, we use a statistical model called spatial point process (SPP). We assume three types of SPPs, namely homogeneous Poisson process (HPP), inhomogeneous Poisson process (IPP) and Poisson cluster process (PCP) [68, 69]. A majority of user distributions in real scenarios can be described accurately with the help of these three SPP models. Let D denote a bounded set, $X(D)$ denote a counting measure of D which calculates the random number of points in D, and $\mu(D)$ is a mean measure of D, giving the expected number of points.

2.5.1 Homogeneous Poisson process (HPP)

When HPP is applied, all user points are uniformly and independently distributed within the target area W. We denote the point density which describes the average number of user points in a unit area as λ_s. Therefore, we have constant λ_s in HPP

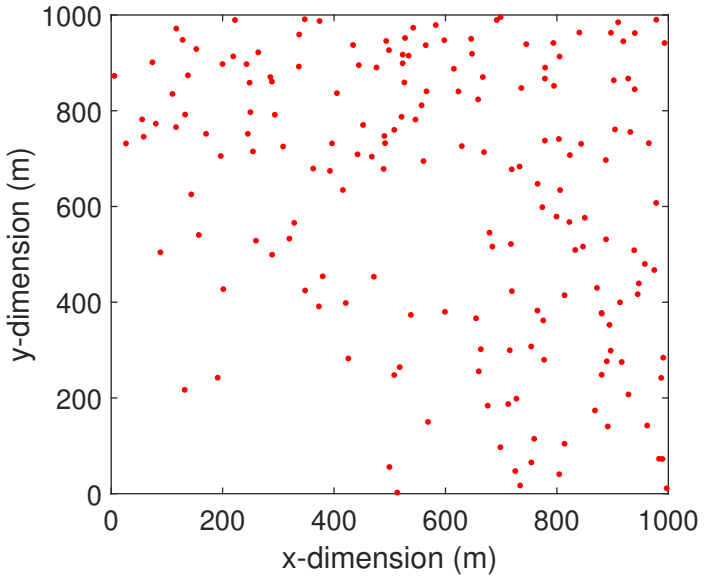

Figure 2.4: An example of user points following IPP with $\lambda(x,y) = 300(x^2+y^2)$

and any user (x_i, y_i) generated with HPP follows

$$P((x_i, y_i) \in S) = \frac{S}{W} \tag{2.9}$$

for any subarea S of the target area W. Note that the number of generated user points follows Poisson distribution, which is $X(D) \sim \text{Poisson}(\lambda_s \cdot W)$. The expected number of points is given by $\mu(D) = \lambda_s \cdot W$. An example of user points distributed following HPP is shown in Fig. 2.3.

2.5.2 Inhomogeneous Poisson process (IPP)

In some cases, grounds users are distributed unevenly, with users in some areas located more densely than other areas. Correspondingly, we need a more general SPP model which introduces inhomogeneity. When IPP is applied, the constant point density λ_s is replaced by an intensity function $\lambda(x,y)$, which varies with locations in the target area. Correspondingly, we have

$$\mu(D) = E\{X(D)\} = \int_D \lambda(x,y)dxdy \tag{2.10}$$

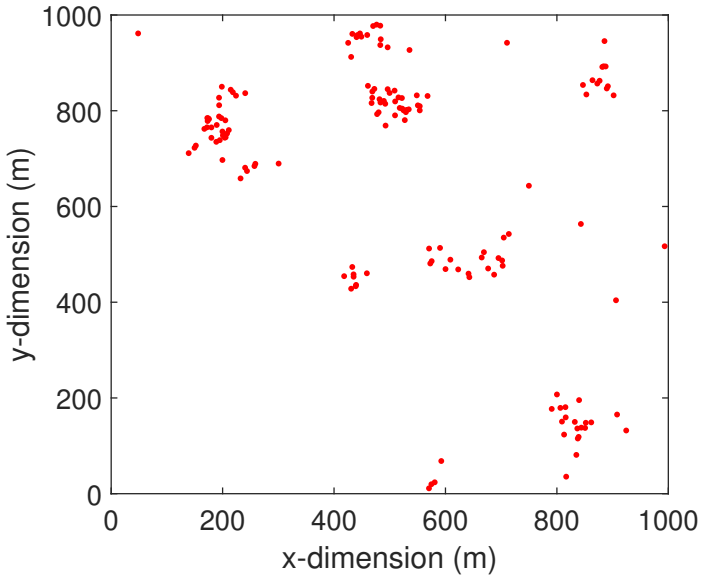

Figure 2.5: An example of user points following PCP with $\lambda_p = 10$

where $E\{.\}$ is the expectation operator. The corresponding number of generated user points is thus $X(D) \sim \text{Poisson}(\mu(D))$, with $\mu(D)$ obtained from (2.10). Note that various intensity function leads to various patterns of ground users. Fig. 2.4 shows an example of ground users generated with

$$\lambda(x,y) = 300(x^2 + y^2) \tag{2.11}$$

It can be seen that, with such a density function, less users are located in the left bottom corner.

2.5.3 Poisson cluster process (PCP)

In practice, ground users often gather around points of interest such as concert and stadium, in which case their distributions involves clustering. In order to describe this kind of user distribution, PCP is utilized [69]. For applying PCP, a set of *parent* points S_p is first generated following HPP with constant point density λ_p. Then for each $c \in S_p$, *children* points which are also known as *offspring* points are independently generated following Poisson process with intensity function $\lambda_c(x,y)$. In this case, *children* points are distributed in circles around corresponding *parent* points to form clusters. Fig. 2.5 shows an example of generated user points with $\lambda_p = 10$

users/km^2 and the *children* points generated with

$$\lambda_c(x,y) = \frac{\alpha}{2\pi\sigma^2} e^{-\frac{1}{2\sigma^2}(x^2+y^2)} \tag{2.12}$$

where $\alpha = 0.9$ and $\sigma = 0.02$. Note that for all the SPPs, *Simplicity* property is satisfied, which means the generated points never coincide [69].

Chapter 3

UAVs Serving as Static Aerial BSs

3.1 Introduction

As mentioned in Chapter 1, the priority of static aerial BSs is finding the optimal locations of UAVs so that the aerial BSs can cover a maximum number of ground users. This is relevant in emergency scenarios such as search-and-rescue after natural disasters and rural area scenarios where there is no ground infrastructures. Meanwhile, since UAVs usually use built-in batteries for supplying power, limited on-board energy is another key factor that limits the lifetime of aerial BSs [11, 56–58].

In this chapter, we study the efficient deployment of multiple UAVs so the maximum user coverage probability is achieved while avoiding the effect of ICI. Following [48, 49], we assume that the UAVs have the knowledge of ULI with the help of high-accuracy GPS systems and each aerial BS has enough capacity to supply all the users within its coverage area. We further assume that the ground users have low mobility. We consider a practical scenario where multiple aerial BSs are deployed in a target area without the service of ground BSs. Note that this is relevant in rural area coverage in cases where terrestrial BSs are absent, and in natural disaster scenarios where terrestrial infrastructures are damaged. Rotary-wing UAVs are chosen as the carrier for static aerial BSs since they have the ability to hold still in the air as well as move in arbitrary directions [11]. The UAV placement problem is modelled as a circle placement problem and the ICI is avoided

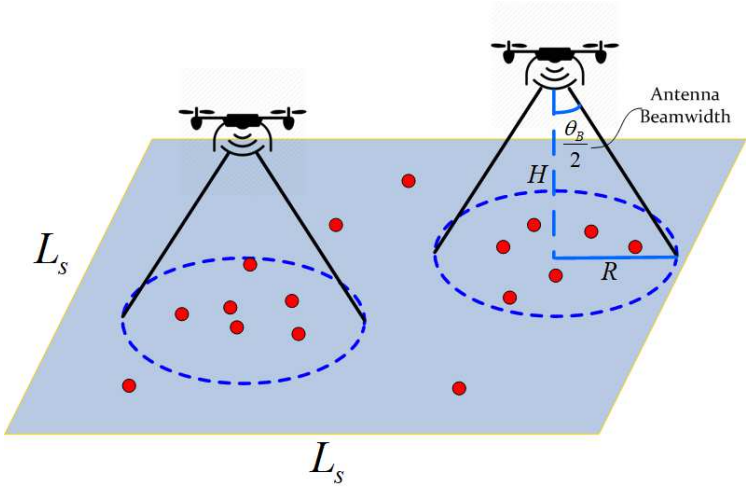

Figure 3.1: System model

by allowing no coverage overlap. Three different deployment methods are proposed successively, and our simulation results demonstrate that the proposed circle placement methods achieve better user coverage performance than the benchmark technique. Furthermore, when the simultaneous deployment methods are applied, the increased coverage probability is achieved with significantly reduced transmit power in certain scenarios. We finally consider the existence of inaccurate ULI and propose a robust technique to compensate the performance loss.

3.2 System Model

We consider a square geographical target area with side length L_s containing a set of low-mobility users denoted by $\mathscr{M}$ as shown in Fig. 3.1. We assume a total of K aerial BSs are deployed within the region in order to provide wireless coverage to as many ground users as possible. Note that, due to the mobility of UAVs, such deployment of aerial BSs can be done regularly in order to accommodate any changes in the user positions. Since static aerial BSs are considered, we will only focus on each snapshot of users within the area instead of studying the trajectory of UAVs. We assume that each aerial BS is equipped with a single directional antenna, and the half-power beamwidth of the antenna is denoted as θ_B. Following the work [29,48],

the antenna gain can be approximated by

$$G = \begin{cases} G_0, -\frac{\theta_B}{2} \leq \phi \leq \frac{\theta_B}{2}, \\ g(\phi), \text{otherwise}, \end{cases} \tag{3.1}$$

where $G_0 \approx \frac{29000}{{\theta_B}^2}$ is the main lobe gain of the directional antenna. For simplicity, we assume the power gain outside of the main lobe is negligible, that is $g(\phi) \approx 0$. We denote the location of user i in the set $\mathscr{M}$ as (x_i, y_i), the horizontal location and the altitude of the k-th UAV as (x_{ck}, y_{ck}) and h_k, $k = 1, 2, ...K$ respectively. Therefore, the ground distance between the i-th user and the k-th UAV is $l_{ik} = \sqrt{(x_i - x_{ck})^2 + (y_i - y_{ck})^2}$. In addition, the coverage area of the k-th aerial BS can be approximated as a circle region centered at (x_{ck}, y_{ck}), with radius $R_k = h_k \tan\left(\frac{\theta_B}{2}\right)$, and the i-th user is covered by the k-th aerial BS when $l_{ik} \leq R_k$.

For ease of exposition, and following [24, 49, 53], we assume that the AtG communication channels are dominated by LoS links. In fact, recent field experiments carried out by Qualcomm have verified that the AtG channels are indeed dominated by the LoS links [70] and the high probability of LoS links is one of the main reasons that motivates us to deploy aerial BSs. Under the LoS models, we have negligible small-scale fadings, and the channel quality depends only on the distance between UAVs and users, which follows FSPL model given by

$$\text{PL}_{ik} = 20 \log\left(\frac{4\pi f_c d_{ik}}{c}\right) \tag{3.2}$$

where c denotes the light speed and f_c denotes the carrier frequency of the system. Additionally, d_{ik} represents the Euclidean distance between user i and the k-th aerial BS, which is given by

$$d_{ik} = \sqrt{{l_{ik}}^2 + {h_k}^2} \tag{3.3}$$

As mentioned in the previous chapter, the service threshold of a BS is defined in terms of the received power. We denote the received power of user i as P_r^i. If the transmit power of the k-th aerial BS is denoted by P_t^k, P_r^i in dB is given by

$$P_r^i = P_t^k + G - \text{PL}_{ik} \tag{3.4}$$

It can be seen from (3.4) that the users located on the border of the circle coverage area will suffer more severe path loss than other covered users. More importantly, the received power of any user who is covered by the aerial BS should be larger than or equal to the threshold value $P_{\min}$. Therefore, aerial BSs which are deployed at a higher altitude require an increased transmit power. Note that when multiple aerial BSs are deployed, the effect of ICI needs to be addressed. With the use of directional antennas and following the LoS channel model, it can be found that the interference effect can be intrinsically avoided when there is no overlap between coverage areas of aerial BSs.

3.3 Proposed Deployment Methods

In this section, we introduce the proposed deployment methods for achieving the best coverage performance based on the system model introduced above. The first proposed technique deploys the UAVs in a successive way while the other two techniques simultaneously deploy all the aerial BSs with the help of K-means clustering. Note that, the third technique can be regarded as a advanced method of the second technique, which further improves the coverage probability while increasing the endurance of aerial BSs.

3.3.1 Successive Deployment Method with Geometrical Relaxation (SD-GR)

We first propose a method based on successive circle placement to find the optimal locations of aerial BSs such that a maximum number of ground users can be covered. Following [48], and as shown in Fig. 3.1, we assume that all UAVs have the same antenna beamwidth θ_B and are flying at a fixed altitude H. Correspondingly, all the aerial BSs have the same coverage radius R, that is

$$\begin{aligned} &h_k = H, k = 1,2,...,K \\ &R_k = R, k = 1,2,...,K \\ &R = H\tan(\frac{\theta_B}{2}) \end{aligned} \tag{3.5}$$

Therefore, deploying multiple aerial BSs is equivalent to placing multiple circles in the horizontal plane such that the number of enclosed user points is maximized. UAVs are placed in a successive method, where at each step the placement of the aerial BS aims to cover the maximum number of remaining users in the target area while ensuring that there is no overlap in coverage areas with all previously deployed BSs. The first aerial BS can be placed with the method proposed in [47]. We denote the coverage area of the first UAV as C_1 and define an integer variable $u_i \in \{0,1\}$, $i \in \mathscr{M}$ denoting the coverage status of user i. To be specific, the i-th user is enclosed by C_1 when $u_i = 1$ and is out of the coverage area of the first UAV when $u_i = 0$. Then the circle placement problem is formulated as

$$\begin{aligned} &\underset{x_{c1},y_{c1},u_i}{\text{maximize}} \sum_{i\in\mathscr{M}} u_i \\ &\text{subject to} \\ &(x_i - x_{c1})^2 + (y_i - y_{c1})^2 \leq R^2 + M(1-u_i), \forall i \in \mathscr{M} \\ &u_i \in \{0,1\}, \forall i \in \mathscr{M} \end{aligned} \tag{3.6}$$

where (x_{c1}, y_{c1}) is the horizontal location of the first UAV, i.e. the center of the coverage region, and M is a constant that can be any value larger than the square of the largest distance between any two points in the target area. It can be observed that the first constraint of (3.6) reduces to

$$(x_i - x_{c1})^2 + (y_i - y_{c1})^2 \leq R^2, \forall i \in \mathscr{M} \tag{3.7}$$

when $u_i = 1$ which is equivalent to saying that the i-th user is covered by the first UAV, and the objective function of (3.6) is increased by 1 correspondingly. In addition, when $u_i = 0$, the very large constant M ensures that any choice of (x_{c1}, y_{c1}) within the target area will satisfy the first constraint of (3.6) [47]. This time we have $u_i = 0$, and the i-th user is not covered by the aerial BS and the value of the objective function keeps the same.

When we want to deploy the second UAV, we need an additional constraint

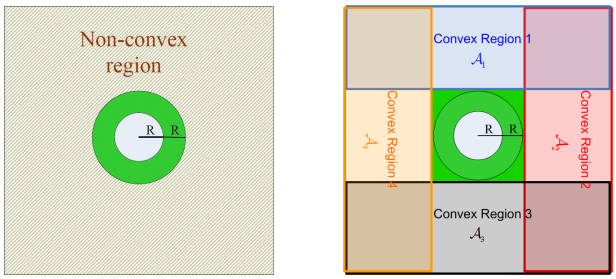

(a) non-convex region (b) four convex regions

Figure 3.2: Converting the non-convex region into convex regions with geometrical relaxation

ensuring no overlap between coverage areas, and thus no ICI. To satisfy this constraint, the distance between the two UAVs in the horizontal dimension should be no smaller than $2R$. Therefore, the placement of the second UAV is formulated as

$$\begin{aligned} &\underset{x_{c2},y_{c2},u_i}{\text{maximize}} \sum_{i\in\mathscr{M}} u_i \\ &\text{subject to} \\ &(x_i - x_{c2})^2 + (y_i - y_{c2})^2 \leq R^2 + M(1-u_i), \forall i \in \mathscr{M} \\ &(x_{c2} - x_{c1})^2 + (y_{c2} - y_{c1})^2 \geq 4R^2 \\ &u_i \in \{0,1\}, \forall i \in \mathscr{M} \end{aligned} \tag{3.8}$$

where (x_{c2}, y_{c2}) is the horizontal location of the second UAV. Unfortunately, the additional constraint is non-convex which makes (3.8) extremely difficult to solve. Although the boolean variables can be tackled with advanced mixed integer programming techniques, using solvers such as MOSEK and Gurobi [47], the optimization problem (3.8) which is a MINLP with non-convex constraint is hardly to be straightforwardly solved. Even if we apply semidefinite relaxation (SDR) techniques to convert the quadratic programs into the form of semidefinite matrix which makes the non-convex constraint of (3.8) convex, a problem with both integer variables and positive semidefinite matrix is still unsolvable with existing tools [71].

In Fig. 3.2(a), the coverage area of the first aerial BS is represented by the circle in white with radius R, and the green circle with radius $2R$ represents the area where there cannot be any placement of additional UAVs without inflicting

ICI. Accordingly, the whole region outside the green circle is the geometrical representation of the second constraint in (3.8). One main observation is that such a non-convex region which specifies all the feasible locations of the second UAV in the horizontal dimension can be divided into four linear regions which are convex. This is done by approximating the green circular area by a square area as illustrated in Fig. 3.2(b). With this approximation, the effective area for placing the second UAV is slightly decreased by $(16-4\pi)R^2$. Therefore, instead of solving (3.8), we can solve four MINLP problems with different linear constraints. Each of the four problems has the following form

$$\begin{aligned}
&\underset{x_{c2},y_{c2},u_i}{\text{maximize}} \sum_{i\in\mathscr{M}} u_i \\
&\text{subject to} \\
&(x_i-x_{c2})^2+(y_i-y_{c2})^2 \le R^2+M(1-u_i), \forall i \in \mathscr{M} \\
&y_{c2} \ge y_{c1}+2R, \text{if } (x_{c2},y_{c2}) \in \mathscr{A}_1 \\
&x_{c2} \le x_{c1}-2R, \text{if } (x_{c2},y_{c2}) \in \mathscr{A}_2 \\
&y_{c2} \le y_{c1}-2R, \text{if } (x_{c2},y_{c2}) \in \mathscr{A}_3 \\
&x_{c2} \ge x_{c1}+2R, \text{if } (x_{c2},y_{c2}) \in \mathscr{A}_4 \\
&u_i \in \{0,1\}, \forall i \in \mathscr{M}
\end{aligned} \tag{3.9}$$

where $\mathscr{A}_1$, $\mathscr{A}_2$, $\mathscr{A}_3$ and $\mathscr{A}_4$ are the four convex regions shown in Fig. 3.2(b). The maximum number of covered users as well as the location of the second UAV is then found among the results of four MINLP problems. Note that the overlap between the four convex regions will not affect the final result and is thus allowed. If the optimal location of the second UAV is inside the overlapping area, it is expected that two of the four optimization problems will give the same solution which contains a maximum number of covered users.

More generally, the optimization problem of placing the k-th UAV ($k > 1$) can

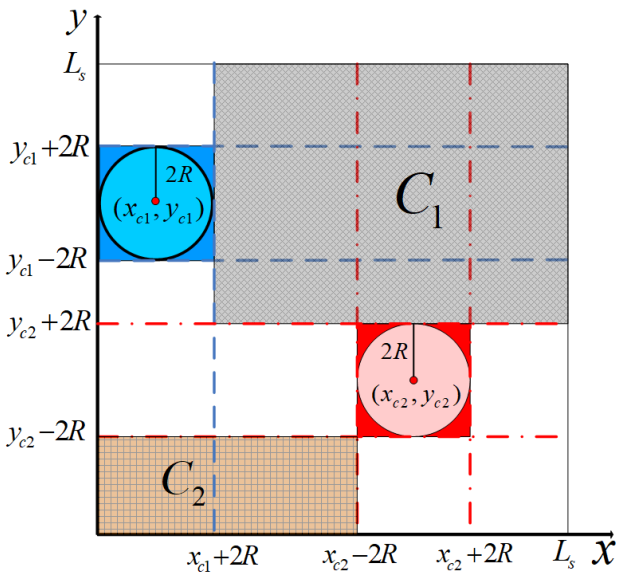

Figure 3.3: An example of feasible region definition, with two deployed aerial BSs, for the positioning of the third BS

be formulated as

$$\begin{aligned}
&\underset{x_{ck},y_{ck},u_i}{\text{maximize}} \sum_{i\in\mathscr{M}} u_i \qquad (3.10)\\
&\text{subject to}\\
&(x_i-x_{ck})^2+(y_i-y_{ck})^2 \le R^2+M(1-u_i), \forall i\in\mathscr{M}\\
&(x_{ck}-x_{cj})^2+(y_{ck}-y_{cj})^2 \ge 4R^2, j=1,2,\ldots,k-1\\
&u_i\in\{0,1\}, \forall i\in\mathscr{M}
\end{aligned}$$

where (x_{ck},y_{ck}) and (x_{cj},y_{cj}) denote the horizontal location of the k-th UAV and the j-th UAV respectively. For each of the $k-1$ non-convex constraints, we use geometrical relaxation to convert it into four linear constraints as illustrated above. Note that the four convex regions with regard to the j-th aerial BS only specify the areas avoiding ICI between the k-th and j-th aerial BSs. In order to find the feasible regions which guarantee no ICI between the k-th aerial BS and all the previously deployed aerial BSs, we need to find all possible intersections of $(k-1)$ convex areas. To be specific, for each of the previously deployed $k-1$ UAVs, one of the four generated feasible regions is selected and we apply logic function to find the intersec-

tion of these $k-1$ selected regions to make sure the coverage area of the next aerial BS does not interfere with any previously deployed aerial BSs. A total of 4^{k-1} intersections should be generated and we denote each intersection as $C_z, z = 1,2,...,4^{k-1}$. The total number of feasible convex regions depends on specific deployment but can be found through an elimination method. Specifically, after obtaining all the 4^{k-1} intersections, we eliminate all sets which are null sets, i.e. $C_z = \emptyset$ or sets which turn out to be subsets of other generated sets, i.e. $C_z \subseteq C_q, q = 1,2,...,4^{k-1}, q \neq z$, and the remaining intersections are the feasible regions we should search for. An example of obtaining feasible regions for placing the third aerial BS is shown in Fig. 3.3, where the horizontal center of the third UAV is denoted by (x_{c3}, y_{c3}). The region C_1 is formed by taking the intersection of $\{x_{c3}, y_{c3} | x_{c1} + 2R \leq x_{c3} \leq L_s, 0 \leq y_{c3} \leq L_s\}$ which is one of the convex regions with regard to the first aerial BS, and $\{x_{c3}, y_{c3} | 0 \leq x_{c3} \leq L_s, y_{c2} + 2R \leq y_{c3} \leq L_s\}$ which is one of the convex regions associated with the second UAV. Therefore, region C_1 is one of the feasible regions we should search for. Another region C_2, however, turns out to be a subset of another generated region $\{x_{c3}, y_{c3} | 0 \leq x_{c3} \leq L_s, 0 \leq y_{c3} \leq y_{c2} - 2R\}$, and is thereby eliminated. We denote the total number of feasible regions for deploying the k-th UAV as N_M^k. Therefore, solving problem (3.10) is equivalent to solve N_M^k MINLP problems, each has the following form

$$
\begin{aligned}
&\underset{x_{ck}^m, y_{ck}^m, u_i}{\text{maximize}} \sum_{i \in \mathscr{M}} u_i \\
&\text{subject to} \\
&(x_i - x_{ck}^m)^2 + (y_i - y_{ck}^m)^2 \leq R^2 + M(1 - u_i), \forall i \in \mathscr{M} \\
&(x_{ck}^m, y_{ck}^m) \in C_k^m \\
&u_i \in \{0,1\}, \forall i \in \mathscr{M}
\end{aligned}
\tag{3.11}
$$

where C_k^m denotes the m-th feasible region of the k-th aerial BS and (x_{ck}^m, y_{ck}^m) is the optimal location of the k-th UAV in region C_k^m, $m = 1,2,...,N_M^k$. If we denote the number of covered users by solving the m-th optimization problem as N_m, and denote the maximum N_m for all m as $N_{\max}$, we have $(x_{ck}, y_{ck}) = (x_{ck}^m, y_{ck}^m)|_{N_m = N_{\max}}$.

Algorithm 1 Algorithm for placing the k-th UAV with geometrical relaxation

Inputs: user locations, $(x_i, y_i) \in \mathscr{M}$; radius of coverage area, R; locations of all deployed UAVs $(x_{cj}, y_{cj}), j = 1, 2, ..., k-1$

Output: number of users covered by the k-th UAV, U_k; the location of the k-th UAV, (x_{ck}, y_{ck})

Initialization: j=1; z=1; m=0.

while $j < k$ **do**
  converting the constraint $(x_{ck} - x_{cj})^2 + (y_{ck} - y_{cj})^2 \geq 4R^2$ into four linear constraints which are $x_{ck} \geq x_{cj} + 2R$, $x_{ck} \leq x_{cj} - 2R$, $y_{ck} \geq y_{cj} + 2R$, and $y_{ck} \leq y_{cj} - 2R$ respectively.
  $j = j + 1$.
end while
For each of the $k-1$ UAVs, one of the four linear constraints is selected to form the intersection of these $k-1$ regions. A total of 4^{k-1} intersections are generated and denoted as $C_z, z = 1, 2, ..., 4^{k-1}$.
while $z < 4^{k-1}$ **do**
  if $C_z = \emptyset$ **then**
    eliminate C_z
  else if $C_z \subseteq C_q, q = 1, 2, ..., 4^{k-1}, q \neq z$ **then**
    eliminate C_z
  else
    $m = m + 1$, $C_k^m = C_z$.
    obtain (x_{ck}^m, y_{ck}^m), and N_m by solving (3.11)
  end if
  $z = z + 1$.
end while
$N_{\max} = \max(N_m), U_k$=$N_{\max}, m = 1, 2, ..., N_M^k$.
$(x_{ck}, y_{ck}) = (x_{ck}^m, y_{ck}^m)|_{N_m = N_{\max}}$.

In addition, $U_k = N_{\max}$, where U_k denotes the number of covered users by the k-th aerial BS. For clarity, the proposed geometrical relaxation method is summarized in Algorithm 1.

3.3.2 Simultaneous Deployment Method with K-means Clustering (SD-KM)

The drawback of the SD-GR technique is that it introduces exponentially increasing computational complexity which requires to solve 4^{k-1} logic combination operations for the optimal deployment of the k-th UAV. When it is required to deploy a large number of aerial BSs, the use of SD-GR becomes prohibitively complex. As a

result, there is a strong motivation for seeking a method which significantly reduces the computational complexity. In this section, we propose a method which deploys multiple aerial BSs at the same time with the help of clustering technique.

K-means clustering might be the most famous partitional clustering method and has been widely used in a variety of disciplines [72]. In our particular scenario, we observe that the whole target area can be divided into K subareas with boundaries forming the Voronoi diagram, by applying K-means clustering. The intelligent division of the target area brings great benefit to the deployment of multiple aerial BSs in several senses. First, each subarea which is bounded by few line segments or straight lines is a polygon region and hence a convex region. Within each convex region, we can efficiently solve an optimization problem similarly to (3.6) to find the best location of a UAV so a maximum number of ground users within that subarea is covered. In addition, the boundary lines ensure that the circle coverage areas placed in each subarea will not overlap with each other, so the ICI is intrinsically avoided. Furthermore, the optimal location of the k aerial BSs can be simultaneously found within their corresponding subareas, so the latency and dependence on previously deployed aerial BSs with SD-GR method is solved. Last but not the least, applying K-means clustering is able to find potential clustering properties among user points. The clustering properties give us a hint about how many aerial BSs we should deploy in the target area, so we can cover a maximum number of ground users without deploying inadequate or excessive UAVs. The details of the proposed SD-KM technique are introduced in the following two subsections.

3.3.2.1 Applying K-means clustering and partitioning the target area

We assume the user set $\mathscr{M}$ contains a total of U_{tot} users and we denote arrays storing the location of user points by $\mathbf{w}_i$, where $\mathbf{w}_i = [x_i, y_i]$, $i = 1, 2, ..., U_{\text{tot}}$. By applying K-means clustering, U_{tot} user points are assigned into K clusters $\mathscr{C}_k$, $k \in [1, K]$, with the k-th cluster, $k = 1, 2, ..., K$, containing N_k user points, out of which $U_k \leq N_k$ users are covered by the corresponding aerial BS. The partition of user points is based on

the sum-of-squared-error criterion [72] which is defined as

$$e = \sum_{k=1}^{K} \sum_{i=1}^{U_{\text{tot}}} u_{ki} \|\mathbf{w}_i - \mathbf{m}_k\|^2 \tag{3.12}$$

where u_{ki} is an integer variable, indicating whether i-th user is assigned into the k-th cluster. To be specific, we have $u_{ki} = 1$ when $\mathbf{w}_i \in \mathscr{C}_k$ and $u_{ki} = 0$ otherwise. $\mathbf{m}_k$ here denotes an array storing the center location of the k-th cluster. Note that the center location of a certain cluster is calculated as the mean value of all user points classified into that cluster, which can be written as

$$\mathbf{m}_k = [m_{kx}, m_{ky}] = \left\{ \frac{1}{N_k} \sum_{i=1}^{U_{\text{tot}}} u_{ki} x_i, \frac{1}{N_k} \sum_{i=1}^{U_{\text{tot}}} u_{ki} y_i \right\} \tag{3.13}$$

where $k = 1, 2, ..., K$. Then the procedure of applying the K-means clustering is concluded in the following steps.

1. Randomly choose K points in the target area as the center locations of the K clusters and store the locations in $\mathbf{m}_k$

2. Allocate each user point in $\mathscr{M}$ to the cluster with the closest center $\mathscr{C}_j$, i.e., $(x_i, y_i) \in \mathscr{C}_j$ when the Euclidean distance between $\mathbf{w}_i$ and the center of cluster j is smaller than the Euclidean distance between $\mathbf{w}_i$ and any other cluster centers.

$$\begin{aligned} &\left\|\mathbf{w}_i - \mathbf{m}_j\right\| < \|\mathbf{w}_i - \mathbf{m}_k\|, \\ &i = 1, 2, ..., U_{\text{tot}},\ k = 1, 2, ..., K,\ j \neq k \end{aligned} \tag{3.14}$$

3. Recalculate the mean position of all user points in each cluster and the center location of the corresponding cluster is updated with the mean position value.

4. Repeat step 2 and step 3 until the change in $\mathbf{m}_k$ is below a certain threshold value.

Note that K-means clustering can only be applied when we have knowledge about how many clusters we want to form, which is not true for our case. Either excessive or inadequate number of generated subareas may deteriorate the coverage performance. Note that the number of required clusters highly depends on user distributions, so it is expected to utilize variable K value in different scenarios. For all cases, we first start with a maximum K value, denoted as $K_{\max}$, making sure adequate number of subareas are generated even for the case showing the least clustering property, i.e., user points following uniform distribution. Then we apply an iterative algorithm to determine the most suitable K value. As excessive partition can split a single cluster into several parts, which severely deteriorate the performance of the proposed method, we set a threshold d_{th} indicating the minimum allowed distance between two cluster centers. To be specific, $\min(\left\|\mathbf{m}_j - \mathbf{m}_k\right\|) < d_{th}$, $j \neq k$ signifies that some of the generated clusters are too small as a result of using too large K value. Correspondingly, we reduce the value of K by one and reapply the K-means clustering. The above procedure continues until we have $\min(\left\|\mathbf{m}_j - \mathbf{m}_k\right\|) \geq d_{th}$ and the iteration ends.

3.3.2.2 Solving optimization problem within each region

After partitioning the user points into K clusters and, subsequently, dividing the whole target area into K subareas, we first need to find the largest allowed coverage area within each subarea to avoid interference. Due to the uncertainty of user distribution and the polygon shape of each subarea, it is likely that certain subareas can only accommodate circles with radii smaller than R. Assume the k-th subarea is formed with S_k line segments or straight lines, each line is expressed in the form of $y = a_{kl}x + b_{kl}$, $l = 1, 2, ..., S_k$, where a_{kl} and b_{kl} denote the slope and offset of the l-th boundary line of the k-th subarea respectively. It is known that for any point (x_d, y_d), if $y_d - a_{kl}x_d - b_{kl} < 0$, the point locates in the halfspace below the line. On the contrary, if $y_d - a_{kl}x_d - b_{kl} > 0$, the point locates in the other halfspace above the line [73]. Note that the distance between the circle center and each boundary line should be no smaller than the length of radius of the circle coverage area. Therefore,

the region for placing the circle can be obtained by shifting the boundary lines of each subarea. If the cluster center $\mathbf{m}_k$ is in the region below a certain boundary line of the k-th subarea, the corresponding new line specifying the region for placing the circle center can be found by shifting the line downward along the y-axis by L_{kl}. Similarly, shifting the original boundary line upward along the y-axis by L_{kl} leads to the corresponding new line when $\mathbf{m}_k$ is in the region above the original boundary line. Here, L_{kl} denotes the length to be shifted along the y-axis of the l-th boundary line of the k-th subarea, and is calculated through

$$L_{kl} = \frac{R^k_{\max}}{\cos(|a_{kl}|)},\ k = 1,2,...,K,\ l = 1,2,...,S_k \tag{3.15}$$

where $R^k_{\max}$ denotes the maximum allowed radius of the circle placed in the k-th subarea. Therefore, $R^k_{\max}$ can be found by solving the following optimization problem.

$$\begin{aligned}
&\underset{x_{ck},y_{ck},R^k_{\max}}{\text{maximize}}\ R^k_{\max} \\
&\text{subject to} \\
&y_{ck} - a_{kl}x_{ck} - b_{kl} + L_{kl} \le 0, \\
&\text{if } m_{ky} - a_{kl}m_{kx} - b_{kl} \le 0 \\
&y_{ck} - a_{kl}x_{ck} - b_{kl} - L_{kl} \ge 0, \\
&\text{if } m_{ky} - a_{kl}m_{kx} - b_{kl} \ge 0 \\
&k = 1,2,...,K,\ l = 1,2,...,S_k
\end{aligned} \tag{3.16}$$

After obtaining $R^k_{\max}$, the radius of the k-th circle is calculated as $R_k = \min(R, R^k_{\max})$. With given radii, we can then find the optimal placement of aerial BSs within their corresponding subareas. With the help of K-means clustering, we can simultane-

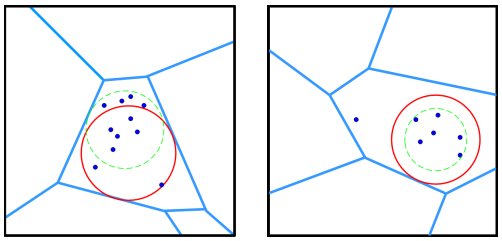

(a) (b)

Figure 3.4: The case for optimizing the radius in K-means circle placement algorithm: (a) flexibility in reaching additional users, (b) reducing power for a given user coverage area.

ously solve K optimization problems of the following type

$$\begin{aligned}
&\underset{x_{ck},y_{ck},u_i}{\text{maximize}} \sum_{i\in\mathscr{M}} u_i \qquad (3.17)\\
&\text{subject to}\\
&(x_i - x_{ck})^2 + (y_i - y_{ck})^2 \le {R_k}^2 + M(1-u_i), \forall i \in \mathscr{M}\\
&y_{ck} - a_{kl}x_{ck} - b_{kl} + \frac{R_k}{\cos(|a_{kl}|)} \le 0,\\
&\text{if } m_{ky} - a_{kl}m_{kx} - b_{kl} \le 0\\
&y_{ck} - a_{kl}x_{ck} - b_{kl} - \frac{R_k}{\cos(|a_{kl}|)} \ge 0,\\
&\text{if } m_{ky} - a_{kl}m_{kx} - b_{kl} \ge 0\\
&u_i \in \{0,1\}, \forall i \in \mathscr{M}\\
&k = 1,2,...,K,\ l = 1,2,...,S_k
\end{aligned}$$

The above optimization problem is a MINLP problem without non-convex constraints and is nearly as easy to solve as (3.6). Note that $K < K_{\max}$ is obtained in most cases as illustrated in the previous subsection.

3.3.3 Energy Efficient Simultaneous Deployment Method with Variable Radius (SD-KMVR)

In the preceding section, we propose a simultaneous deployment method which divides the whole target area into K convex subareas, so we can solve multiple convex

optimization problems at the same time. However, the proposed SD-KM technique can be further improved in terms of both the coverage performance and power consumption. A key observation is that maximum allowed circle coverage area does not always lead to maximum number of covered ground users within an irregular polygon region. As can be seen in Fig. 3.4(a), user points may gather in a relative narrow region where circles with large radii can not reach, and more users can thus be enclosed when we shrink the coverage area. In other words, further improved coverage performance can be achieved with variable size of coverage area. Moreover, since there might be no user points located right on the border of the coverage areas, the radii of circle areas and hence the transmit power of aerial BSs can be further reduced. It can be seen in Fig. 3.4(b) that, the original coverage area in red obtained by the SD-KM technique can be shrunk into the green coverage area which covers the same set of user points with a reduced transmit power.

In order to address the above mentioned problems, we further propose an iterative algorithm in this section. We assume each aerial BS has a minimum allowed coverage area with radius $R_{\min}$, then the radius of the k-th coverage area r_k has a range of $R_{\min} \leq r_k \leq R_k$. First, we find the circle center (x_{ck}, y_{ck}) as well as the set containing the covered user points, denoted as $\mathscr{M}_{\text{cov}}^k$ with size U_k by solving (3.17) with radius R_k. Then, with fixed center location (x_{ck}, y_{ck}), we find the minimum r_k which is able to enclose the same set of user points $\mathscr{M}_{\text{cov}}^k$ by solving the following problem,

$$
\begin{aligned}
&\text{minimize } r_k \\
&\text{subject to} \\
&{r_k}^2 \geq (x_i - x_{ck})^2 + (y_i - y_{ck})^2, \forall i \in \mathscr{M}_{\text{cov}}^k \\
&R_{\min} \leq r_k \leq R_k
\end{aligned}
\tag{3.18}
$$

After obtaining r_k, we replace R_k with r_k and solve (3.17) again to find the updated user points covered by the new circle area. The above procedure repeats until the radius r_k does not change anymore. For brevity, we summarize the iterative algo-

Algorithm 2 Iterative algorithm for placing the k-th UAV

Inputs: Initial radius R_k; an intermediate value storing the change of radius, r_{it}.
Output: Set containing all covered user points, $\mathscr{M}_{\text{cov}}^k$; the location of the k-th UAV, (x_{ck}, y_{ck}); the optimal radius r_k.
Initialization: $r_{it} = 0$, $r_k = R_k$
1: **while** $r_{it} \neq r_k$ **do**
2: $r_{it} = r_k$
3: obtain (x_{ck}, y_{ck}) and $\mathscr{M}_{\text{cov}}^k$ by solving (3.17) and replacing R_k with r_{it}.
4: obtain r_k by solving (3.18).
5: **end while**

rithm in Algorithm 2. Moreover, as the size of coverage areas are shrunk and all the aerial BSs have the same antenna beamwidth θ_B, the altitude of the k-th UAV can be found by

$$h_k = \frac{r_k}{\tan\left(\frac{\theta_B}{2}\right)} \tag{3.19}$$

We hence mark the 3-D location of the k-th aerial BS as (x_{ck}, y_{ck}, h_k). Furthermore, the reduced radii also reduce the communication path loss according to (3.4) and thus reduce the required transmit power of aerial BSs since we have

$$P_t^k = P_{\min} + \text{PL}(r_k) - G \tag{3.20}$$

where P_t^k is the required transmit power of the k-th aerial BS. Note that $P_{\min}$ is the threshold valve of received transmit power as defined in the second section of this chapter, below which the communication link is failed. The total required power of the system can thus be found by summarizing the transmit power of all aerial BSs as follows

$$P_{total} = \sum_{k=1}^{K} P_t^k = K(P_{\min} - G) + \sum_{k=1}^{K} \text{PL}(r_k) \tag{3.21}$$

It is clear that the total required power is a function of both r_k and K.

3.4 Imperfect ULI and Robust Deployment

In practice, it is difficult to obtain perfect ULI. As a result, the coverage performance of the proposed techniques may decrease drastically. In this section, we propose a

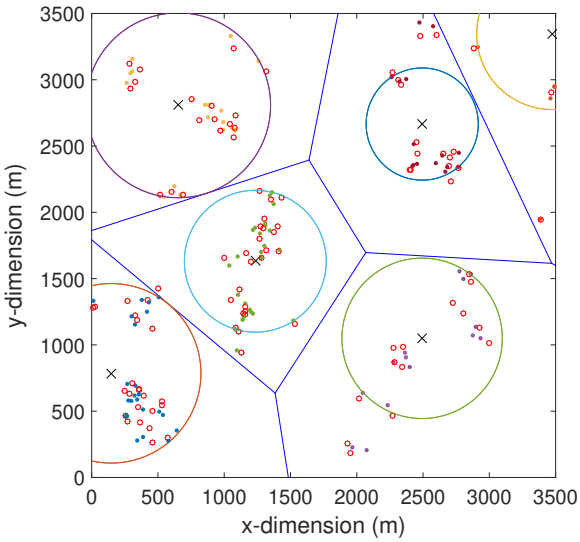

Figure 3.5: An example deployment of SD-KMVR in the existence of imperfect ULI, with dots representing estimated user locations and small circles in red representing real user locations.

robust technique which is applicable to both SD-KM and SD-KMVR to preserve the best coverage performance in the existence of imperfect ULI. We denote the estimated location of the i-th user by $(\widetilde{x_i}, \widetilde{y_i}) = (x_i + e_{xi}, y_i + e_{yi})$, where e_{xi} and e_{yi} are estimation errors following Gaussian distribution with zero mean and standard deviation σ in meters. For ease of illustration, we show an example deployment of SD-KMVR in the existence of imperfect ULI with $\sigma = 50$ m and $L_s = 3.5$ Km in Fig. 3.5. The SD-KMVR technique is applied based on estimated ULI represented by dots, while real user locations are represented by small circles in red. It can be seen that, user points which are closer to the horizontal centers of aerial BSs have better immunity to estimation errors. The coverage probability declines when the user points which are considered to be enclosed are actually out of the coverage range of the corresponding aerial BSs.

Intuitively, increased robustness against inaccurate ULI can be achieved with a larger size of coverage area. We assume the maximum deviation between real location and estimated location for any ground user is d_{th}, where $d_{th} \approx 3\sigma$. Therefore, the performance loss of coverage probability for the k-th aerial BS can be

Algorithm 3 Robust deployment of aerial BSs

Inputs: Placement details obtained from SD-KM or SD-KMVR technique: radius of coverage areas, R_k; horizontal location of aerial BSs, (x_{ck}, y_{ck}); location of covered user points, $(x_i, y_i), \forall i \in \mathscr{M}_{\text{cov}}^k$

Output: New horizontal location of aerial BSs, (x_{ck}^*, y_{ck}^*); new radius of coverage areas, R_k^*.

1: Find the minimum distance between (x_{ck}, y_{ck}) and the boundary lines of the corresponding subarea.
2: Obtain (x_{ck}^*, y_{ck}^*) by solving (3.24).
3: Calculate the minimum distance between (x_{ck}^*, y_{ck}^*) and the boundary lines of the corresponding subarea.
4: Obtain R_k^* from (3.25).

completely compensated when

$$L_{\text{min}}^k = |R_k - r_{ik}| \geq d_{th}, \forall i \in \mathscr{M}_{\text{cov}}^k \tag{3.22}$$

where L_{min}^k denotes the minimum difference between r_{ik} and R_k of the k-th subarea. As can be seen in the preceding section, increasing the radii of coverage areas also increases the required transmit power and thus decreases the endurance of aerial BSs. Correspondingly, there is a trade-off between robustness against imperfect ULI and required transmit power with regard to the radius. Therefore, the aim of the robust design, which is maximizing the number of covered user points in the existence of imperfect ULI, is equivalent to maximizing L_{min}^k with minimum transmit power. In addition, we observe that the user points are usually distributed unevenly within the corresponding coverage area for both SD-KM and SD-KMVR techniques. In this case, some ground users have a much larger ground distance to the aerial BS than the rest of ground users within the subarea. Therefore, relocating the center of aerial BS to minimize the maximum ground distance between the center location and the user points covered by the aerial BS can reduce the resulting radius and thus reduce the required transmit power. We denote the distance between (x_{ck}, y_{ck}) and the boundary lines of the corresponding subarea as $d_{kl}, l = 1, 2, ..., S_k$. Then the minimum value among all the S_k distances is $d_{\text{min}}^k = \min(d_{kl})$. In order to avoid ICI, we should only relocate the horizontal center of the k-th aerial BS within

a circular area with radius $d^k_{\min}$. Therefore, the corresponding optimization problem is formulated as

$$\begin{aligned} &\underset{x^*_{ck},y^*_{ck}}{\text{minimize}} \max_{i\in M^k_{\text{cov}}} \left(\sqrt{(x^*_{ck}-x_i)^2+(y^*_{ck}-y_i)^2}\right) \\ &\text{subject to} \\ &\sqrt{(x^*_{ck}-x_{ck})^2+(y^*_{ck}-y_{ck})^2} \le d^k_{\min} \\ &k=1,2,...,K \end{aligned} \tag{3.23}$$

where (x^*_{ck}, y^*_{ck}) denotes the new center of the k-th aerial BS in the horizontal dimension, and is the variable to optimize. (x_{ck}, y_{ck}) is the horizontal center location obtained by either SD-KM or SD-KMVR. Note that the objective function of (3.23) implicitly includes the constraint that all the originally covered ground users are still covered. The above optimization problem is equivalent to minimizing an auxiliary variable d_k representing the maximum ground distance between k-th aerial BS and the user points it covered as follows

$$\begin{aligned} &\underset{x^*_{ck},y^*_{ck}}{\text{minimize}}\, d_k \\ &\text{subject to} \\ &\sqrt{(x^*_{ck}-x_i)^2+(y^*_{ck}-y_i)^2} \le d_k, i\in M^k_{\text{cov}} \\ &\sqrt{(x^*_{ck}-x_{ck})^2+(y^*_{ck}-y_{ck})^2} \le d^k_{\min} \\ &k=1,2,...,K \end{aligned} \tag{3.24}$$

After obtaining the new horizontal center location (x^*_{ck}, y^*_{ck}), we recalculate the minimum ground distance between the k-th aerial BS and the corresponding boundary lines and denote it as $d^{k^*}_{\min}$. Then the maximum allowed radius within the k-th subarea is calculated as $R^{k^*}_{\max} = \min(R, R_k + d^{k^*}_{\min})$. The radius of the k-th coverage area R^*_k can be obtained by

$$R^*_k = \begin{cases} d_k + d_{th}, \text{if } d_k + d_{th} \le \mathrm{R}^{k^*}_{\max} \\ \mathrm{R}^{k^*}_{\max}, \text{if } d_k + d_{th} > \mathrm{R}^{k^*}_{\max} \end{cases} \tag{3.25}$$

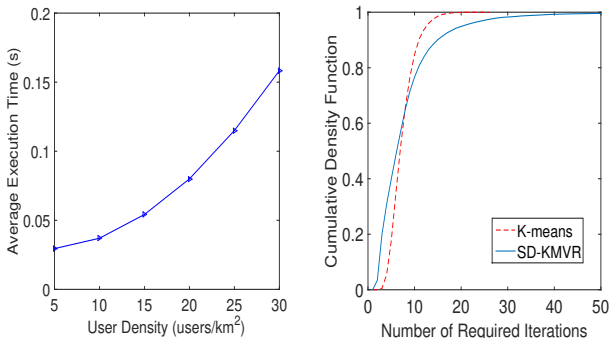

(a) (b)

Figure 3.6: Computational complexity: (a) average execution time of solving a single MINLP problem by MOSEK solver, $K = 1$; (b) CDF of number of iterations required for K-means clustering and SD-KMVR, $K = 9$, $\lambda_s = 10$ users/km^2

Note that the radius R_k^* is not necessarily larger than R_k, especially when the robust technique is applied to SD-KM. In other words, we can sometimes obtain a further reduced transmit power with the proposed robust technique. For clarity, we summarize the procedure of applying the robust technique in Algorithm 3.

3.5 Computational Complexity

In this section, we study the computational complexity of the proposed techniques in terms of the number of floating-point operations. Following [73, 74], the computational costs are calculated based on real-valued additions, subtractions, multiplications, divisions and comparisons.

3.5.1 Complexity of SD-GR

For deploying the k-th aerial BS ($k > 2$), we first need to find a total of 4^{k-1} candidate sets. Each of the 4^{k-1} sets is an intersection of $k-1$ sets, and forming each intersection needs $4(k-2)$ comparisons in the worst case for both x and y dimensions. Therefore, the complexity of finding the candidate regions for deploying a total of K aerial BSs needs $\sum_{k=3}^{K} 2(k-2)4^k$ floating-point operations, which can be simplified as

$$C_{GR}^{1} = \mathcal{O}\{\frac{16K-14}{9} \cdot 4^{K+1}\} \tag{3.26}$$

In the elimination process, the complexity comes from checking the feasibility of all candidate sets. Since there are $\sum_{k=2}^{K} 4^{K-1}$ candidate sets in total, the resulting computational complexity is

$$C_{GR}^{2} = \mathscr{O}\{\frac{1}{3} \cdot 4^{K+1}\} \tag{3.27}$$

It is in general difficult to determine the average complexity of solving (3.11), since it does not have a closed form solution. Note that the complexity of solving (3.11) is involved in all the deployment schemes, so we denote it as C_{MINLP} and represent the complexity of all techniques as a function of C_{MINLP}. As a result, the total computational complexity for SD-GR technique is

$$\begin{aligned} C_{GR} &= C_{GR}^{1} + C_{GR}^{2} + KC_{\text{MINLP}} \\ &= \mathscr{O}\{\frac{6K-11}{9} \cdot 4^{K+1}\} + KC_{\text{MINLP}} \end{aligned} \tag{3.28}$$

To characterize the complexity of solving a single MINLP, we employ the average execution time against various user density as shown in Fig. 3.6(a).

3.5.2 Complexity of SD-KM

The complexity of K-means clustering takes an important part in the overall complexity of SD-KM. Here, the average number of iterations of K-means clustering is denoted by n_{it} and cumulative distribution function (CDF) describing the convergence for K-means clustering is shown as the dashed line in Fig. 3.6(b). Three steps are involved within each iteration of K-means clustering. In first step, the Euclidean distance between each user point and cluster centers is calculated, which involves two multiplications, two subtractions, one addition and one square root. Therefore, for a scenario with U_{tot} ground users and K aerial BSs, calculating all Euclidean distances requires $\mathscr{O}\{6KU_{\text{tot}}\}$ floating-point operations. The second step allocates each user point to the closest cluster. This step needs $\mathscr{O}\{U_{\text{tot}}(K-1)\}$ comparisons in total. Finally, we need to recalculate the cluster centers following (3.13), which includes U_{tot} multiplications, $U_{\text{tot}}-1$ additions and one division for both x and y

dimensions. Then the costs for the third stage is $O\{4KU_{\text{tot}}\}$. Therefore, the overall computational complexity of k-means clustering is

$$\mathscr{O}\{n_{\text{it}}(6KU_{\text{tot}} + U_{\text{tot}}(K-1) + 4KU_{\text{tot}})\} \approx \mathscr{O}\{KU_{\text{tot}}n_{\text{it}}\} \tag{3.29}$$

For applying SD-KM we also need to find a reasonable K value, and the proposed iterative algorithm repeats all the calculations shown above for N_{KM} times until $\min(\|\mathbf{m}_j - \mathbf{m}_k\|) \geq d_{th}$. Correspondingly, we have

$$C^1_{\text{KM}} = \mathscr{O}\{N_{\text{KM}}KU_{\text{tot}}n_{\text{it}}\} \tag{3.30}$$

Furthermore, we need to find the maximum allowed radius within each subarea according to (3.16). Following [75], (3.16) is a convex problem solved by interior-point methods and has the following computational complexity

$$C_{\text{IP}} = \mathscr{O}\{(E+F)^{1.5}E^2\} \tag{3.31}$$

where E is the number of variables, and F is the number of constraints involved in the optimization problem. In our specific scheme, we have S_k constraints and 3 variables for solving the k-th optimization problem, so the costs of finding all the maximum allowed radius is given by

$$C^2_{\text{KM}} \approx \mathscr{O}\{\sum_{k=1}^{K}(3+S_k)^{1.5}\} \tag{3.32}$$

The computational complexity of solving (3.17) is again approximated by C_{MINLP}. Accordingly, the total computational complexity of SD-KM technique is

$$\begin{aligned} C_{\text{KM}} &= C^1_{\text{KM}} + C^2_{\text{KM}} + KC_{\text{MINLP}} \\ &= \mathscr{O}\{N_{\text{KM}}KU_{\text{tot}}n_{\text{it}} + \sum_{k=1}^{K}(3+S_k)^{1.5}\} \\ &\quad + KC_{\text{MINLP}} \end{aligned} \tag{3.33}$$

3.5.3 Complexity of SD-KMVR

The SD-KMVR technique can be regraded as an advanced version of SD-KM technique and involves all operations of SD-KM. Besides, SD-KMVR includes additional computational costs for finding the appropriate coverage radius. We first note that SD-KMVR is an iterative algorithm, and we denote the average number of required iterations as $n_{\text{it}}^{\text{vr}}$. In addition, CDF of the number of required iterations for SD-KMVR technique is shown as the blue straight lines in Fig. 3.6(b). Within each iteration, we need to solve (3.17) with a complexity of C_{MINLP} and (3.18). Since the number of constraints of (3.18) is U_k, the costs of solving (3.18) is $\mathscr{O}\{\sum_{k=1}^{K}(U_k+1)^{1.5}\}$. Therefore, the overall computational complexity of SD-KMVR technique is

$$\begin{aligned} C_{\text{KMVR}} &= C_{\text{KM}} + \mathscr{O}\{n_{\text{it}}^{\text{vr}} \sum_{k=1}^{K}(U_k+1)^{1.5}\} \\ &\quad + n_{\text{it}}^{\text{vr}} K C_{\text{MINLP}} \\ &= \mathscr{O}\{N_{\text{KM}} K U_{\text{tot}} n_{\text{it}} + \sum_{k=1}^{K}(1+S_k)^{1.5} + \\ &\quad n_{\text{it}}^{\text{vr}} \sum_{k=1}^{K}(U_k+1)^{1.5}\} + (n_{\text{it}}^{\text{vr}}+1) K C_{\text{MINLP}} \end{aligned} \tag{3.34}$$

3.5.4 Complexity of Robust Technique

Compared to SD-KM and SD-KMVR, the additional computational complexity of applying the robust technique arises from (3.23), which is again solved by interior-point method. With regard to (3.23), we have $E = 2$ and $F = U_k + K - 1$, so the computational cost is

$$C_{\text{robust}} \approx \mathscr{O}\{\sum_{k=1}^{K} U_k + K^2\} \tag{3.35}$$

For clarity, the computational complexity of all the proposed techniques is summarized in Table 3.1. Note that the benchmark CPT is originally designed for maximizing the coverage area instead of maximizing the number of covered users. Therefore, by applying CPT, the location of aerial BSs is fixed for a specific target area, and the technique has negligible complexity.

Table 3.1: Computational Complexity of the Proposed Techniques

Method	Computational costs
SD-GR	$\mathcal{O}\{\frac{6K-11}{9}\cdot 4^{K+1}\}+KC_{\text{MINLP}}$
SD-KM	$\mathcal{O}\{N_{\text{KM}}KU_{\text{tot}}n_{\text{it}}+\sum_{k=1}^{K}(3+S_k)^{1.5}\}+KC_{\text{MINLP}}$
SD-KMVR	$\mathcal{O}\{N_{\text{KM}}KU_{\text{tot}}n_{\text{it}}+\sum_{k=1}^{K}(3+S_k)^{1.5}$ $+n_{\text{it}}^{\text{vr}}\sum_{k=1}^{K}(U_k+1)^{1.5}\}+(n_{\text{it}}^{\text{vr}}+1)KC_{\text{MINLP}}$
Robust SD-KM	$\mathcal{O}\{N_{\text{KM}}KU_{\text{tot}}n_{\text{it}}+\sum_{k=1}^{K}(3+S_k)^{1.5}\}$ $+KC_{\text{MINLP}}+\mathcal{O}\{\sum_{k=1}^{K}U_k+K^2\}$
Robust SD-KMVR	$\mathcal{O}\{N_{\text{KM}}KU_{\text{tot}}n_{\text{it}}+\sum_{k=1}^{K}(3+S_k)^{1.5}$ $+n_{\text{it}}^{\text{vr}}\sum_{k=1}^{K}(U_k+1)^{1.5}\}+(n_{\text{it}}^{\text{vr}}+1)KC_{\text{MINLP}}$ $+\mathcal{O}\{\sum_{k=1}^{K}U_k+K^2\}$

3.6 Simulation Results

In this section, we assume multiple aerial BSs are vertically deployed with the same antenna beamwidth. Therefore, with the parameters shown in Table 3.2, the radius R corresponds to a received power threshold $P_{\min}=-67$ dBm is calculated as R= 707 m. We assume the minimum allowed radius of coverage area and the minimum allowed distance between two clusters are $R_{\min}=\frac{R}{2}$ and $d_{th}=\frac{R}{2}$ respectively. The value of $K_{\max}$ is set as the same value as the number of circles resulting from CPT. Without loss of generality, we utilize three different SPPs to modele the user distribution, which are HPP with λ_s= 5 users/km^2, IPP with $\lambda(x,y)=5(x^2+y^2)$ users/km^2 and PCP respectively. The *parent* points of PCP are generated following HPP with $\lambda_p=1$ users/km^2 and the *children* points are generated with

$$\lambda_c(x,y)=\frac{\alpha}{2\pi\sigma^2}e^{-\frac{1}{2\sigma^2}(x^2+y^2)} \tag{3.36}$$

Table 3.2: Simulation parameters1

parameter	f_c	c	θ_B	P_t
value	2.5 Ghz	$3 \cdot 10^8$ m/s	95°	30 dBm

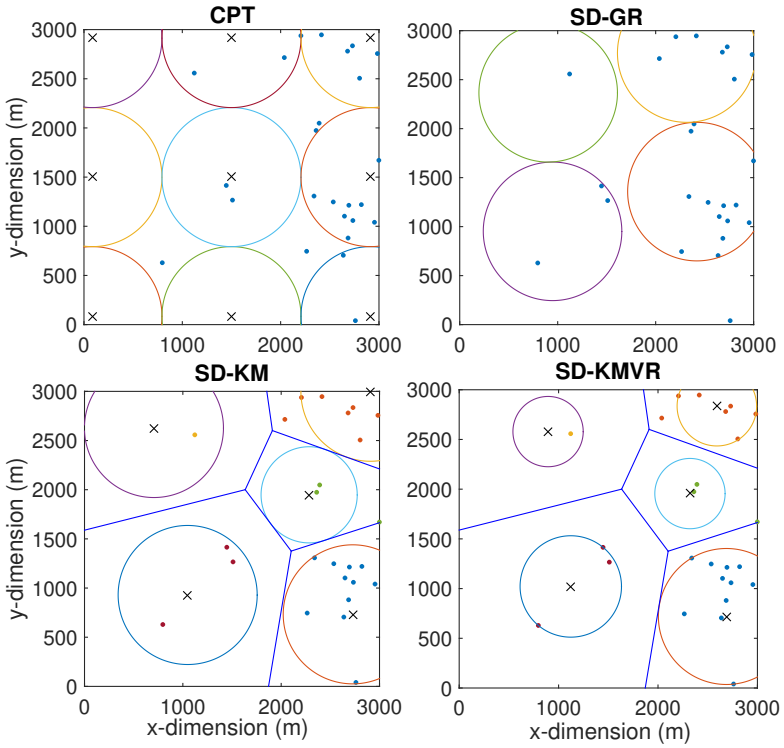

Figure 3.7: Aerial BS placement with proposed techniques

where $\alpha = 0.9$ and $\sigma = 0.02$. The details of the above SPPs have been introduced in Chapter 2. To evaluate the benefit of the proposed techniques, numerical results based on Monte Carlo simulations of the proposed SD-GR, SD-KM, SD-KMVR and the robust techniques are compared with the performance of CPT which serves as the benchmark. Note that the exponentially increasing computational complexity of SD-GR forbids its use when we have a large number of aerial BSs to deploy. With this reason, the SD-GR technique is only used for simulation when the value of K is no larger than four. The horizontal center of all deployed UAVs must fall inside the target area, and we assume the coverage areas outside the target area will not cause further interference to users outside the targeted area.

To illustrate the proposed techniques, example UAV placement distributions

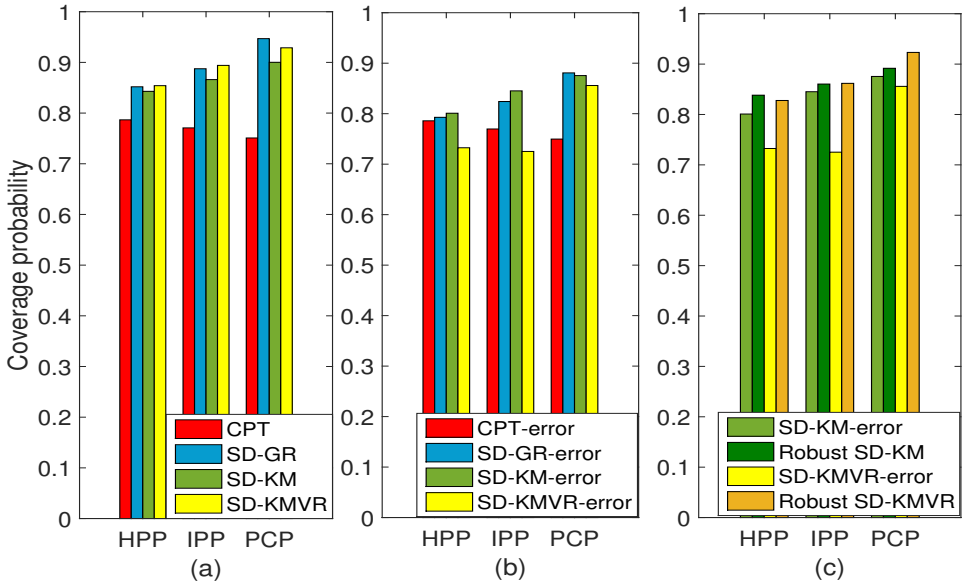

Figure 3.8: User-coverage probability for different types of user distribution: (a) with perfect ULI, (b) with imperfect ULI, (c) with robust technique, K=4

are shown based on simulation for SD-GR, SD-KM, SD-KMVR, and the benchmark CPT in Fig. 7, assuming a PCP distribution of users and $L_s = 3$ km. Note that the CPT simply places circles with same size in a way that maximum coverage area is achieved and none of these circles overlap. For CPT, the number of circles N_{cp} to be placed in a square target area depends on the size of target area, which is represented by $N_{cp} = \lceil \frac{L_s}{2R} \rceil^2$.

3.6.1 Coverage Probability

Intuitively, coverage performance of CPT highly depends on the user distribution. SD-GR method, on the other hand, always aims to cover the most number of user points in the remaining region and is less affected by the specific user distributions. However, the placement of the k-th aerial BS is restricted by the location of previously deployed $k-1$ BSs when SD-GR is applied, which limits the achievable coverage probability.The SD-KM method is able to find the clustering properties among ground users and is thus more robust to the change of user distributions. The coverage performance of SD-KM is limited by the shape of subareas, which may lead to users gathering in a relative narrow region of the subarea uncovered. This drawback is solved by SD-KMVR, which also significantly reduces the required

transmit power and thus increases the endurance of aerial BSs.

The above effects, are captured in Fig. 3.8(a), which illustrates the achieved coverage probability for different types of user distributions. For a fair comparison, a target area with $L_s = 4R$ is assumed, within which all the methods can horizontally deploy a maximum of four circles. It can be clearly seen that the coverage probability of all techniques depends on specific user distributions. Note that the achieved coverage probability of CPT decreases while the performance of all the other techniques increases when the user points tend to have an uneven distribution, especially when clusters are formed. Specifically, the proposed SD-KMVR technique achieves an up to 30% higher coverage performance than CPT when users are following PCP. This result is as expected, since CPT places circles in fixed locations for a given target area no matter how the users are distributed, which highly deteriorate the coverage performance when clusters are formed outside the coverage areas. On the contrary, with the proposed methods, aerial BSs are not deployed at fixed locations, but instead can be flexibly placed according to the change of user distributions.When heterogeneity of user distribution is introduced, ground users are located closer to each other and there is correspondingly a better chance to cover more users within each applied circle coverage area. As can be observed, more than 90% of users are covered with the proposed techniques when users are distributed following PCP.

The coverage performance of the proposed techniques with inaccurate ULI is shown in Fig. 3.8(b). It can be observed that the performance of all the proposed techniques decreases while the performance of CPT remains unchanged in the existence of imperfect ULI. CPT is immune to ULI errors because placement rule of CPT is irrelevant to ULI. Note that SD-KM method shows much better immunity to inaccurate ULI compared to SD-KMVR. This is as expected, since the aerial BSs deployed with SD-KM technique have larger coverage areas causing larger distances between user points and the border of circles. The performance loss in the existence of inaccurate ULI is greatly compensated with the application of proposed

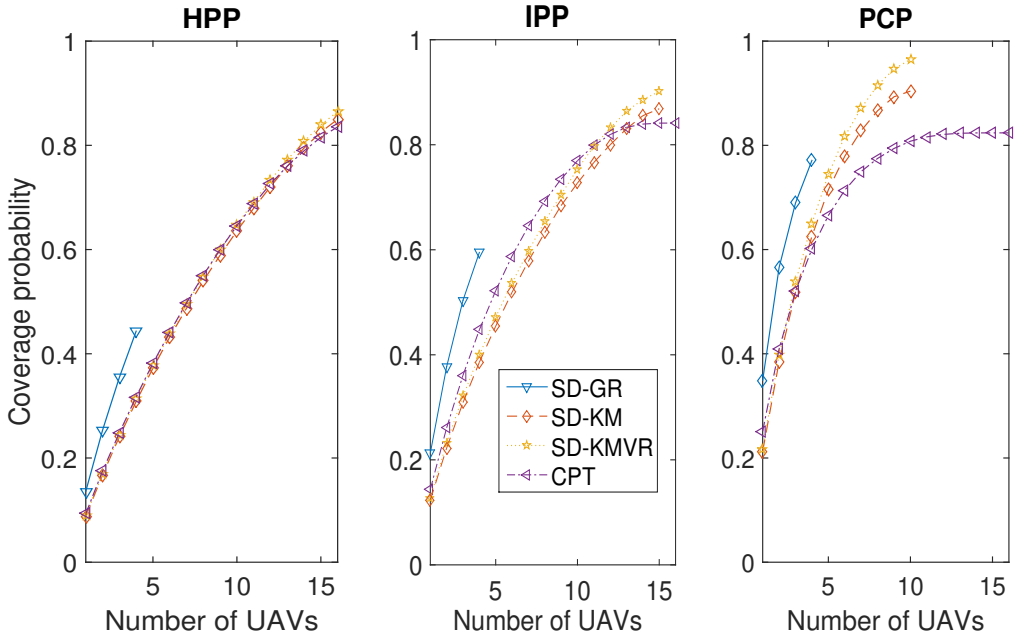

Figure 3.9: User-coverage probability versus number of UAVs deployed, K=16, 15 and 10 for HPP, IPP and PCP correspondingly

robust techniques as shown in Fig. 3.8 (c). The increased coverage performance is achieved thanks to enlarged coverage area as well as relocated coverage centers.

In practice, we may have a limited number of available UAVs for deployment. Therefore, it is of great importance to examine the coverage performance of the proposed methods versus the number of available UAVs. We assume $L_s = 5$ km, the K value used for HPP, IPP and PCP are 16, 15 and 10 respectively, which are the average K values we need for target areas of this size, and the corresponding results are shown in Fig. 3.9. As expected, SD-GR technique significantly outperforms other techniques in all types of user distributions, since the aerial BSs are always deployed to cover the maximum number of users in the remaining areas. It can also be observed that SD-KMVR achieves an up to 10% performance gain compared to SD-KM. SD-KM, SD-KMVR and CPT have comparable performance when users are distributed uniformly, since the K-means clustering method will divide the target area in a similar way as we apply CPT when HPP is followed. When users are distributed following a non-uniform distribution, CPT slightly outperforms the proposed SD-KM and SD-KMVR techniques when we use a small number of aerial BSs. In this case, a similar number of UAVs are deployed in a more tight way than

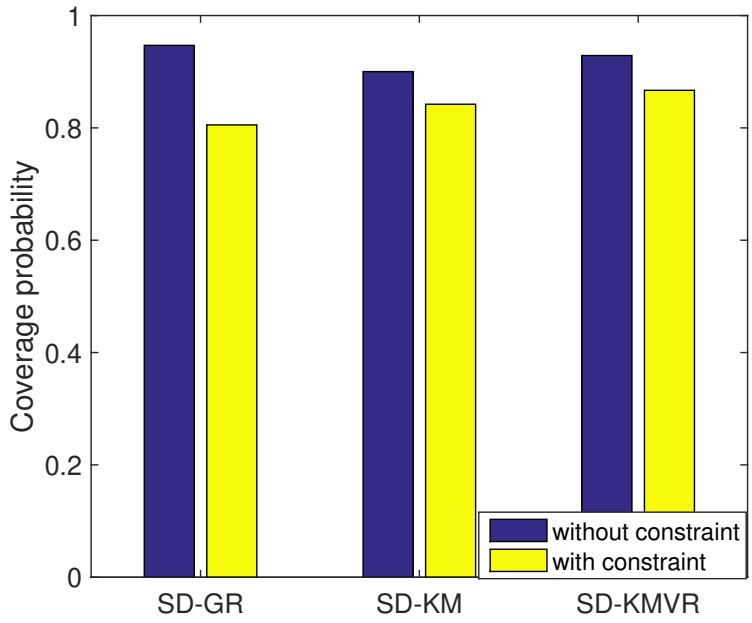

Figure 3.10: Coverage probability with additional constraint specifying the maximum number of served user. $L_s = 4R$.

CPT, causing reduced coverage areas of certain aerial BSs and hence a smaller number of covered users when SD-KM and SD-KMVR are applied. On the contrary, circles placed at positions where the user points are densely located can cover more user points due to the larger coverage area when circle packing technique is used. However, the proposed SD-KM and SD-KMVR techniques regain the superiority when clusters are formed. In this case, aerial BSs are deployed at positions where clustering properties are found.

For real deployment, we have a limited number of users that can be served at the same time due to limited capacity and specific multiplexing methods. In this case, we need to impose an additional constraint specifying the maximum number of served users, i.e., $\sum_{i \in \mathscr{M}} u_i \leq U_{\max}$, where $U_{\max}$ denotes the limitation on the number of users. For comparing the coverage performance of the proposed techniques with and without the additional constraint, we assume the users are distributed following PCP, and $U_{\max} = 30$. As can be seen from Fig. 3.10 , SD-GR suffers the severest performance degradation compared to the other techniques. This is because SD-GR always tries to cover the greatest number of remaining users in the target area, and

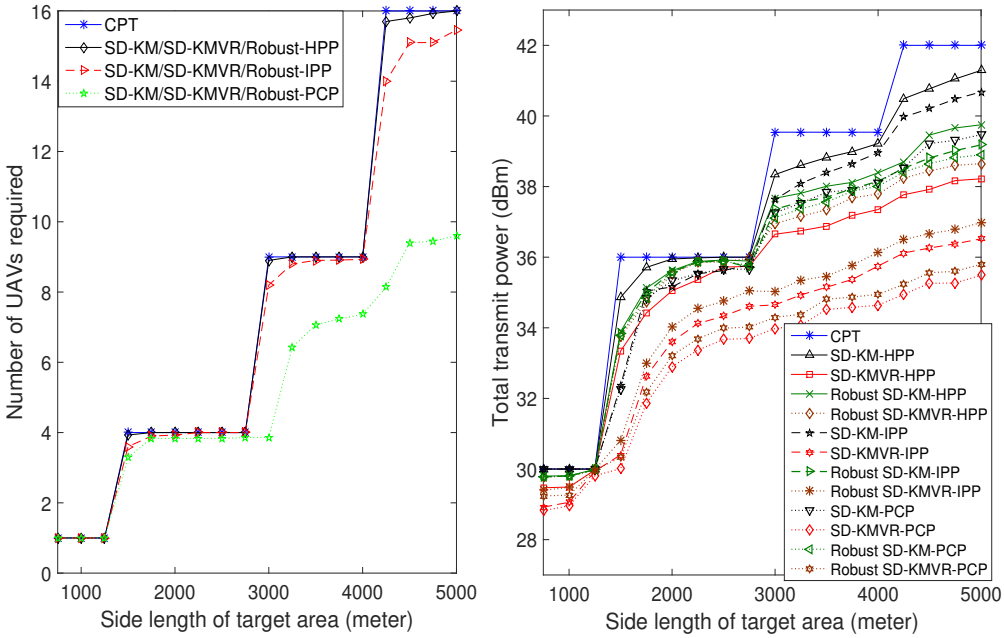

Figure 3.11: Required number of aerial BSs and total transmit power versus size of target area

the deployment of the first few aerial BSs covers a large number of users, which may exceed the threshold.

3.6.2 Energy Efficiency

In Fig. 3.11, we compare the number of required aerial BSs and the required total transmit power for SD-KM, SD-KMVR, Robust SD-KM, Robust SD-KMVR and CPT. It can be seen that, SD-KM and SD-KMVR as well as their robust techniques require a smaller number of aerial BSs compared to CPT when users are distributed unevenly. Furthermore, the gap between the proposed techniques and CPT becomes larger as the size of the target area increases. When $L_s = 5$ km, the number of UAVs required by SD-KM and SD-KMVR is around 60% of that for CPT. In addition, though SD-KM and SD-KMVR require the same number of aerial BSs to be deployed, the SD-KMVR technique is clearly more power-conserving, which saves up to 10% power. Robust SD-KMVR consumes approximately 1% more power than SD-KMVR as a result of increasing the coverage area, but still consumes much less power than SD-KM technique. It is worth highlighting that, Robust SD-KM is even more power efficient than SD-KM. This indicates that, after relocating the circle

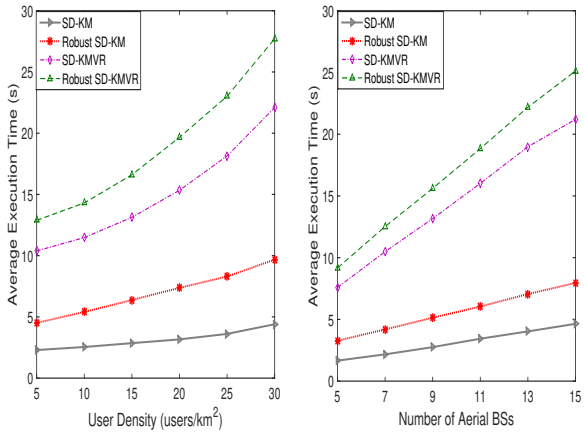

Figure 3.12: Average execution time for the proposed techniques: (a) versus various user density, $K = 9$ (b) versus various number of aerial BSs, $\lambda_s = 5$ users/km^2

center, the minimum distance between covered user points and the border of the corresponding coverage areas is larger than d_{th} in most cases. Note that the reduced number of UAVs saves operation costs and the reduced transmit power can prolong the lifetime of aerial BSs.

3.6.3 Computational Complexity

In Fig. 3.12, we characterize the complexity of SD-KM, SD-KMVR and their robust techniques in terms of the average execution time. The user points are distributed following HPP and an Intel Core i7-6700 2.6GHz CPU computer is used for running the simulation. Fig. 3.12(a) shows the average execution time versus various user densities with K=9, while the average execution time versus various number of UAVs is presented in Fig. 3.12(b) with $\lambda_s = 5$ users/km^2. From both subfigures of Fig. 3.12, it can be seen that, executing SD-KMVR takes more time than SD-KM, and the computational complexity of SD-KMVR increases more faster. Specifically, the execution time of SD-KMVR increases approximately 40% and 105% faster than SD-KM, as the user density and the number of UAVs increase correspondingly. Similar trends is found for Robust SD-KMVR and Robust SD-KM. The results also verify that, the increased robustness is achieved with increased computational complexity, which is consistent with the analytic results shown in section 3.5.4

3.7 Summary

In this chapter, we have investigated the efficient deployment of multiple static aerial BSs in order to maximize the number of covered users while avoiding ICI. Firstly, we propose a successive deployment method which converts each non-convex constraint into four linear constraints with geometrical relaxation. Since the use of SD-GR is prohibitively complex when a large number of aerial BSs are required, we further propose a simultaneous deployment method called SD-KM, which converts the target area into K convex subareas with the help of K-means clustering. Then a simple convex problem can be solved within each subarea. Moreover, an iterative technique is proposed to further improve the coverage performance while increase the endurance of aerial BSs. Finally, for compensating the performance loss in the existence of imperfect ULI, a robust technique which relocates the aerial BSs and adjusts the radii of coverage areas is proposed. Simulation results show that the coverage performance is improved by up to 30% with the proposed methods. Additionally, SD-GR method is the best choice when a small number of UAVs are available, and SD-KMVR saves up to 15% transmit power than SD-KM at a cost of increased computational complexity. Simulation results also verify that the performance loss can be completely compensated with the robust technique when users are distributed unevenly.

Chapter 4

UAVs Serving as Moving Aerial BSs

4.1 Introduction

The focus of this chapter is on flight trajectory and UAV-user scheduling optimization for a moving aerial BS, with the goal of satisfying the data requirement of a maximum number of ground users before exhausting its limited on-board energy. Maximizing the coverage with a given energy budget is the bottom line aim of UAV based aerial BS but is not considered yet. On one hand, moving aerial BS is able to move close to the users to enjoy better communication condition, and thus cover more users within a given time period compared to static aerial BSs. On the other hand, limited on-board energy is a fundamental barrier which constrains the trajectory of the UAV and limits the coverage performance. We assume a user is covered only when the entire data request of the user is satisfied. Same as the previous chapter, we assume that ULI is known with the assistance of high-accuracy GPS systems. Fixed-wing UAVs which have higher speed than roatry-wing UAVs are chosen as the carrier for aerial BSs [11]. The formulated optimization problem is a MINLP with variables closely coupled. To solve the non-convex optimization problem, an iterative algorithm based on alternating optimization method and successive convex optimization is proposed. In addition, to speed up the convergence and improve coverage performance, a new initial trajectory is devised for the iterative algorithm. Finally, as we usually have inaccurate ULI in practice, two different robust techniques are further proposed to compensate for the performance loss.

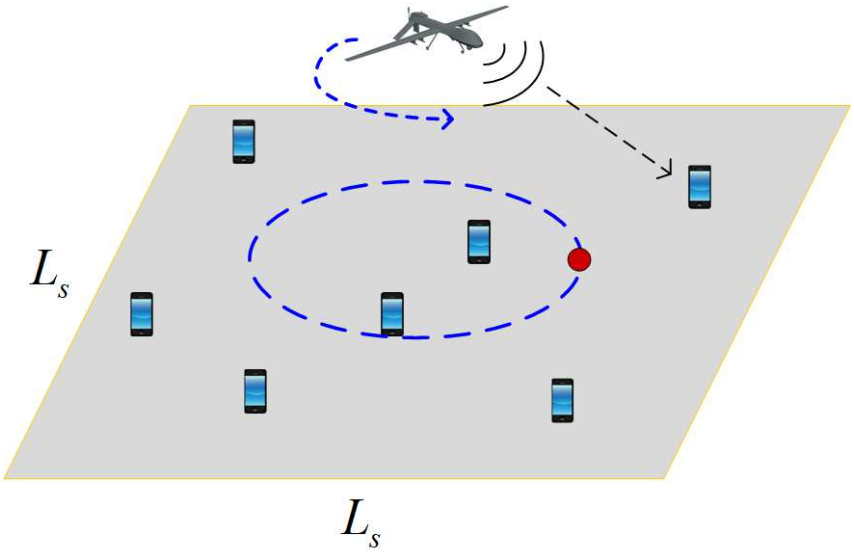

Figure 4.1: Aerial BS serving delay-tolerant users

Simulation results show that a much better coverage performance is achieved with the use of the proposed algorithm.

4.2 System Model

Consistent with Chapter 3, we consider the same square geographical target area of dimension L_s by L_s containing a set of delay-tolerant ground users denoted by $\mathscr{M}$, where $|\mathscr{M}| = M$. We assume the users have low-mobility and are uniformly distributed within the target area. We further assume there exist a perfect backhaul link. Instead of deploying multiple static aerial BSs, we deploy a single moving aerial BS which is able to charge its battery at base, and is represented by the red dot as shown in Fig. 4.1. Within a given time period $T > 0$, the aerial BS is dispatched from base, tring to satisfy the data demand of as many ground users as possible before exhausting its on-board energy and flying back to the base. During any time period, the associated ground users are served via time-division multiple access (TDMA). In practice, we may have multiple backup aerial BSs. We assume the charging time of UAV is T_c, and the number of backup UAVs is N_b. For continuously satisfying the data demand of ground users, we should have $N_b T \geq T_c$. Nevertheless,

in this thesis, we will focus on the coverage performance of a single moving aerial BS within a given mission period T.

We consider a 3-D Cartesian coordinate system where the horizontal location of user i in the set $\mathscr{M}$ is $\mathbf{w}_i = [x_i, y_i]^T \in \mathbb{R}^{2\times 1}$. We assume UAV is flying with a fixed altitude H, where H could correspond to the minimum altitude required for safe operation according to certain policies. For ease of exposition and following [20, 24], we divide the total time period T into N equal time slots, where the time slots are indexed by $n = 1, 2, ..., N$. Furthermore, since TDMA scheme is applied, we assume that the ground users can only be associated at these N time slots. It is required that the time slot length δ_t is efficiently small so the location of the aerial BS changes only slightly within each time slot. Consequently, the trajectory, velocity and acceleration of the UAV are approximated by the following N two-dimensional sequences

$$\mathbf{s}[n] \triangleq \mathbf{s}(n\delta_t) = [s_x[n], s_y[n]]^T, \tag{4.1}$$

$$\mathbf{v}[n] \triangleq \mathbf{v}(n\delta_t) = [v_x[n], v_y[n]]^T, \tag{4.2}$$

$$\mathbf{a}[n] \triangleq \mathbf{a}(n\delta_t) = [a_x[n], a_y[n]]^T, \tag{4.3}$$

$$n = 1, 2, ..., N$$

Moreover, the relationship among $\mathbf{s}[n]$, $\mathbf{v}[n]$ and $\mathbf{a}[n]$ can be described by two equations as follows [24]

$$\mathbf{v}[n+1] = \mathbf{v}[n] + \mathbf{a}[n]\delta_t, \tag{4.4}$$

$$\mathbf{s}[n+1] = \mathbf{s}[n] + \mathbf{v}[n]\delta_t + \frac{1}{2}\mathbf{a}[n]{\delta_t}^2, \tag{4.5}$$

$$n = 1, 2, ..., N-1$$

For simplicity, we again assume the AtG links are dominated by LoS channels [49, 76]. Therefore, we have negligible small-scale effects and the channel quality is dominated by the communication distance. The distance from the aerial BS to the

i-th user at time slot n is given by

$$d_i[n] = \sqrt{H^2 + \|\mathbf{s}[n] - \mathbf{w}_i\|^2} \tag{4.6}$$

Correspondingly, the time-varying channel for user i at time slot n is expressed as

$$h_i[n] = \frac{\beta_0}{d_i[n]^2} = \frac{\beta_0}{H^2 + \|\mathbf{s}[n] - \mathbf{w}_i\|^2} \tag{4.7}$$

where we denote the channel power at the reference distance $d_0 = 1$ m as β_0. We define a binary variable $\alpha_i[n]$ indicating the scheduling and association status of user i in time slot n. To be specific, the i-th user is served by the aerial BS at time slot n if $\alpha_i[n] = 1$, and otherwise $\alpha_i[n] = 0$. At any time slot, at most one of the M users is associated with the aerial BS, so we have

$$\sum_{i=1}^{M} \alpha_i[n] \leq 1, \forall n \tag{4.8}$$

Therefore, if user i is associated with the aerial BS at time slot n, the signal-to-noise ratio (SNR) at user i can be expressed as

$$\gamma_i[n] = \frac{P_t \cdot h_i[n]}{\sigma^2} = \frac{P_t \zeta_0}{H^2 + \|\mathbf{s}[n] - \mathbf{w}_i\|^2} \tag{4.9}$$

where P_t, σ^2 and $\zeta_0 = \frac{\beta_0}{\sigma^2}$ denote the transmit power of the aerial BS, noise power and the referenced received SNR respectively. The achievable throughput for user i in the unit of bits is thus given by

$$U_i = \sum_{n=1}^{N} \alpha_i[n] B \log_2(1 + \gamma_i[n]) \tag{4.10}$$

where B denotes the available bandwidth. In general, the total power consumption of the aerial BS consists of two parts, i.e., the power consumed for communication related functions and the power consumed for supporting the movement of UAV. In practice, the propulsion power consumption is much higher than the communication-related power, and we thus consider only the propulsion power

consumption for simplicity [24, 57]. Propulsion power consumption depends on the flying status of UAV, and a theoretical model was derived in [24]. For tractable analysis, we adopt the upper bound of the model, and the total consumed propulsion power is expressed as

$$P_{\mathrm{c}} = \sum_{n=1}^{N} \left(c_1 \|\mathbf{v}[n]\|^3 + \frac{c_2}{\|\mathbf{v}[n]\|}\left(1 + \frac{\|\mathbf{a}[n]\|^2}{g^2}\right)\right) \tag{4.11}$$

where c_1 and c_2 are constant parameters related to the UAV's design, air density, etc., and $g = 9.8\mathrm{m/s}^2$ represents the gravitational acceleration. Correspondingly, the total consumed energy can be expressed as

$$E_{\mathrm{c}} = \sum_{n=1}^{N} \left(c_1 \|\mathbf{v}[n]\|^3 + \frac{c_2}{\|\mathbf{v}[n]\|}\left(1 + \frac{\|\mathbf{a}[n]\|^2}{g^2}\right)\right) \cdot \delta_t \tag{4.12}$$

4.3 Joint Trajectory and UAV-user Scheduling Design

Based on the system model shown above, in this section, we first formulate the optimization problem as a MINLP. The resulting problem involves multiple coupled variables and is challenging to solve. Correspondingly, we propose an iterative algorithm based on successive convex optimization and iterating optimization problem to tackle the non-convex problem. After that, we further devise an initial trajectory in the second subsection to speed up the convergence and improve the coverage performance.

4.3.1 Proposed Iterative Algorithm

Our goal is to satisfy the data demand of a maximum number of ground users with a limited on-board energy by jointly optimizing the UAV trajectory and the UAV-user scheduling variables. To this end, we define a binary variable ρ_i indicating whether the data request of the i-th user is satisfied or not. Specifically, if the data demand of user i is denoted by Q_i, $\rho_i = 1$ when $U_i \geq Q_i$, and otherwise $\rho_i = 0$.

Correspondingly, the optimization problem is formulated as

$$
\begin{aligned}
(\mathrm{P1}): \quad & \underset{\{\alpha_i[n],\mathbf{s}[n],\mathbf{v}[n],\mathbf{a}[n],\rho_i\}}{\text{Maximize}} \sum_{i\in M} \rho_i && \text{(4.13a)}\\
& \text{subject to} \\
& \sum_{n=1}^{N} \alpha_i[n] B \log_2(1+\gamma_i[n]) \geq \rho_i Q_i, \forall i && \text{(4.13b)}\\
& \rho_i \in \{0,1\}, \forall i && \text{(4.13c)}\\
& \alpha_i[n] \in \{0,1\}, \forall n, \forall i && \text{(4.13d)}\\
& \sum_{i=1}^{M} \alpha_i[n] \leq 1, \forall n && \text{(4.13e)}\\
& \sum_{n=1}^{N} (c_1 \|\mathbf{v}[n]\|^3 + \frac{c_2}{\|\mathbf{v}[n]\|}(1+\frac{\|\mathbf{a}[n]\|^2}{g^2})) \cdot \delta_t \leq E_{\text{tot}} && \text{(4.13f)}\\
& \mathbf{s}[n+1] = \mathbf{s}[n] + \mathbf{v}[n]\delta_t + \frac{1}{2}\mathbf{a}[n]{\delta_t}^2, \\
& n = 1,2,...,N-1 && \text{(4.13g)}\\
& \mathbf{v}[n+1] = \mathbf{v}[n] + \mathbf{a}[n]\delta_t, \\
& n = 1,2,...,N-1 && \text{(4.13h)}\\
& \mathbf{s}[0] = \mathbf{s}[N] = \mathbf{s}_0 && \text{(4.13i)}\\
& \mathbf{v}[0] = \mathbf{v}_0 && \text{(4.13j)}\\
& \|\mathbf{v}[n]\| \leq v_{\max}, \forall n && \text{(4.13k)}\\
& \|\mathbf{v}[n]\| \geq v_{\min}, \forall n && \text{(4.13l)}\\
& \|\mathbf{a}[n]\| \leq a_{\max}, \forall n && \text{(4.13m)}
\end{aligned}
$$

where E_{tot} denotes the total on-board energy of the aerial BS, $\mathbf{s}_0$ denotes the location of the base and $\mathbf{v}_0$ denotes the initial velocity. $v_{\max}$, $v_{\min}$ and $a_{\max}$ further denote the maximum allowed speed, minimum required speed and maximum allowed acceleration of UAV respectively. Constraint (4.13b) judges whether the data demand of user i is satisfied. when the achievable total data for user i is equal or larger than the required data Q_i, $\rho_i = 1$ and the objective function is increased by one correspondingly. However, when the request of user i is not fully met, $\rho_i = 0$

and the objective function remains the same. As can be seen in constraint (4.13f), the total consumed energy should be no larger than the on-board energy of the UAV. According to (4.13i), the aerial BS is dispatched from the base, and should fly back to the base for charging at the end of the mission period. Moreover, the mobility of the aerial BS is governed by constraints (4.13k)-(4.13m). Notably, a minimum speed constraint is set since fixed-wing UAVs can not stay stationary in the sky.

Problem P1 is a non-convex MINLP with multiple variables coupled and is challenging to solve. Although the binary variables can be tackled with advanced mixed integer programming techniques, using solvers such as Gurobi and MOSEK [38, 47], constraints (4.13b), (4.13f) and (4.13l) are non-convex and can not be straightforwardly solved. To this end, we propose an efficient iterative algorithm based on alternating optimization method and successive convex optimization to obtain the sub-optimal solution of P1. Define $\mathbf{A} = \{\alpha_i[n], \forall i, \forall n\}$ and $\mathbf{Q} = \{\mathbf{s}[n], \mathbf{v}[n], \mathbf{a}[n], \forall n\}$ as the set associated with user scheduling and the set associated with UAV mobility respectively. For solving P1, we decompose the problem into two sub-problems and alternately optimize the variables in two sets within each iteration. To be specific, with a given UAV trajectory set $\mathbf{Q}$, first sub-problem of P1, which is denoted by P1.1 can be reformulated as

$$
\begin{aligned}
(\text{P1.1}): \quad & \underset{\{\mathbf{A},\rho_i\}}{\text{Maximize}} \sum_{i\in M} \rho_i && (4.14a)\\
& \text{subject to} \\
& \sum_{n=1}^{N} \alpha_i[n] B \log_2(1+\gamma_i[n]) \geq \rho_i Q_i, \forall i && (4.14b)\\
& \rho_i \in \{0,1\}, \forall i && (4.14c)\\
& \alpha_i[n] \in \{0,1\}, \forall n, \forall i && (4.14d)\\
& \sum_{i=1}^{M} \alpha_i[n] \leq 1, \forall n && (4.14e)
\end{aligned}
$$

Note that except the constraints defining the boolean variables, i.e., (4.14c) and (4.14d), P1.1 is a mixed-integer linear problem (MILP) with a linear objective function (4.14a), and linear constraints (4.14b) and (4.14e). Therefore, P1.1 can be efficiently solved with optimization solvers such as Gurobi and MOSEK.

Similarly, by fixing the user scheduling variables $\mathbf{A}$, the UAV trajectory related variables $\mathbf{Q}$ can be optimized by solving the following sub-problem P1.2.

$$
\begin{aligned}
(\text{P1.2}): \quad & \underset{\{\mathbf{Q},\rho_i\}}{\text{Maximize}} \sum_{i\in M} \rho_i && (4.15a)\\
& \text{subject to} \\
& \sum_{n=1}^{N} \alpha_i[n] B \log_2(1+\gamma_i[n]) \geq \rho_i Q_i, \forall i && (4.15b)\\
& \sum_{n=1}^{N} (c_1 \|\mathbf{v}[n]\|^3 + \frac{c_2}{\|\mathbf{v}[n]\|}(1+\frac{\|\mathbf{a}[n]\|^2}{g^2})) \cdot \delta_t \leq E_{\text{tot}} && (4.15c)\\
& \mathbf{s}[n+1] = \mathbf{s}[n] + \mathbf{v}[n]\delta_t + \frac{1}{2}\mathbf{a}[n]{\delta_t}^2, \\
& n = 1,2,...,N-1 && (4.15d)\\
& \mathbf{v}[n+1] = \mathbf{v}[n] + \mathbf{a}[n]\delta_t, \\
& n = 1,2,...,N-1 && (4.15e)\\
& \mathbf{s}[0] = \mathbf{s}[N] = \mathbf{s}_0 && (4.15f)\\
& \mathbf{v}[0] = \mathbf{v}_0 && (4.15g)\\
& \|\mathbf{v}[n]\| \leq v_{\max}, \forall n && (4.15h)\\
& \|\mathbf{v}[n]\| \geq v_{\min}, \forall n && (4.15i)\\
& \|\mathbf{a}[n]\| \leq a_{\max}, \forall n && (4.15j)\\
& \rho_i \in \{0,1\}, \forall i && (4.15k)
\end{aligned}
$$

As can be seen in the above problem, constraints (4.15d)-(4.15g) are linear and constraints (4.15h) and (4.15j) are convex. In addition (4.15k) specifies that ρ_i is an integer variable, and can be tackled with advanced mixed integer programming techniques. Therefore, the difficulty of solving P1.2 lies in constraints (4.15b), (4.15c) and (4.15i), which are all non-convex. The key observation is that, although the left-hand-side (LHS) of constraint (4.15b), which is U_i, is not concave with respect to $\mathbf{s}[n]$, it is convex with respect to $\|\mathbf{s}[n]-\mathbf{w}_i\|^2$. Since any convex function is globally lower-bounded by its first order Taylor expansion at any point [73], we apply successive convex optimization technique to address (4.15b). Specifically,

with a given local UAV location $\{\mathbf{s}_l[n], \forall n\}$, we yield the following lower bound U_i^{lb} for U_i

$$\begin{aligned} U_i &= \sum_{n=1}^{N} \alpha_i[n] B \log_2\left(1 + \frac{P_t \zeta_0}{H^2 + \|\mathbf{s}[n] - \mathbf{w}_i\|^2}\right) \\ &\geq -\sum_{n=1}^{N} \alpha_i[n] B \cdot A_i^l[n] \left(\|\mathbf{s}[n] - \mathbf{w}_i\|^2 - \|\mathbf{s}_l[n] - \mathbf{w}_i\|^2\right) \\ &+ \sum_{n=1}^{N} \alpha_i[n] B \cdot B_i^l[n] \triangleq U_i^{\text{lb}} \end{aligned} \tag{4.16}$$

where $A_i^l[n]$ and $B_i^l[n]$ are constants which are given by

$$A_i^l[n] = \frac{(\log_2 e) P_t \zeta_0}{(H^2 + \|\mathbf{s}_l[n] - \mathbf{w}_i\|^2)(H^2 + \|\mathbf{s}_l[n] - \mathbf{w}_i\|^2 + P_t \zeta_0)} \tag{4.17}$$

$$B_i^l[n] = \log_2\left(1 + \frac{P_t \zeta_0}{H^2 + \|\mathbf{s}_l[n] - \mathbf{w}_i\|^2}\right), \forall n, \forall i \tag{4.18}$$

The equality of (4.16) holds at the point $\mathbf{s}[n] = \mathbf{s}_l[n], \forall n$. By applying the lower bound U_i^{lb}, we reformulate the non-convex constraint (4.15b) as

$$U_i^{\text{lb}} \geq \rho_i Q_i, \forall i \tag{4.19}$$

Since U_i^{lb} is a concave function with respect to $\mathbf{s}[n]$, (4.19) is convex now. Furthermore, for addressing the non-convexity of (4.15c) and (4.15i), we introduce slack variables $\{\tau_n\}$ as in [24, 63], and the corresponding new constraints are

$$\sum_{n=1}^{N} \left(c_1 \|\mathbf{v}[n]\|^3 + \frac{c_2}{\tau_n}\left(1 + \frac{\|\mathbf{a}[n]\|^2}{g^2}\right)\right) \cdot \delta_t \leq E_{\text{tot}} \tag{4.20}$$

$$\tau_n \geq v_{\min}, \forall n \tag{4.21}$$

$$\|\mathbf{v}[n]\|^2 \geq {\tau_n}^2, \forall n \tag{4.22}$$

With the introduced slack variables $\{\tau_n\}$, variable $\mathbf{v}[n]$ and $\mathbf{a}[n]$ are no more coupled, and the LHS of constraint (4.20) is now jointly convex with respect to

$\{\mathbf{v}[n], \mathbf{a}[n], \tau_n\}$. Note that a new non-convex constraint (4.22) is introduced with such a relaxation. Fortunately, a local optimal solution can be obtained by applying successive convex optimization. To be specific, since the LHS of (4.22) is convex and differentiable with respect to $\mathbf{v}[n]$, a lower-bound of $\|\mathbf{v}[n]\|^2$ can be obtained with any given local point $\{\mathbf{v}_l[n], \forall n\}$ by using the first-order Taylor expansion of $\|\mathbf{v}[n]\|^2$ as follows

$$\begin{aligned} &\|\mathbf{v}[n]\|^2 \geq \|\mathbf{v}_l[n]\|^2 + 2\mathbf{v}_l^T[n](\mathbf{v}[n] - \mathbf{v}_l[n]) \\ &\triangleq \psi_{\text{lb}}(\mathbf{v}[n]) \end{aligned} \tag{4.23}$$

where the equality holds at the point $\mathbf{v}[n] = \mathbf{v}_l[n], \forall n$. Therefore, constraint (4.22) can be replaced with the following new convex constraint

$$\psi_{\text{lb}}(\mathbf{v}[n]) \geq {\tau_n}^2, \forall n \tag{4.24}$$

The sub-problem P1.2 can thus be reformulated as

$$\begin{aligned} (\text{P1.2}'): \quad & \underset{\{\mathbf{Q}, \rho_i, \tau_n\}}{\text{Maximize}} \sum_{i \in M} \rho_i && (4.25a) \\ & \text{subject to } (4.15\text{d} - 4.15\text{h}), (4.15\text{j}), (4.15\text{k}) \\ & U_i^{\text{lb}} \geq \rho_i Q_i, \forall i && (4.25b) \\ & \sum_{n=1}^{N} (c_1 \|\mathbf{v}[n]\|^3 + \frac{c_2}{\tau_n}(1 + \frac{\|\mathbf{a}[n]\|^2}{g^2})) \cdot \delta_t \leq E_{\text{tot}} && (4.25c) \\ & \tau_n \geq v_{\min}, \forall n && (4.25d) \\ & \psi_{\text{lb}}(\mathbf{v}[n]) \geq {\tau_n}^2, \forall n && (4.25e) \end{aligned}$$

As all constraints of P1.2′ are convex and the objective function is a MILP, the optimization problem can again be efficiently solved by standard optimization solvers.

Based on the solution of the two sub-problems P1.1 and P1.2′, we propose an iterative algorithm by applying alternating optimization method for solving P1. Specifically, the optimization variables of the original problem are partitioned into

Algorithm 4 Block coordinate descent technique for solving P1

Initialization: Initial the trajectory set $\mathbf{Q}_0$; Let $l = 0$;

1: **repeat**
2: solve problem P1.1 with given $\{\mathbf{Q}_l\}$, and denote the optimal solution as $\{\mathbf{A}_{l+1}\}$
3: solve problem P1.2′ with given $\{\mathbf{A}_{l+1}\}$, and denote the optimal solution as $\{\mathbf{Q}_{l+1}\}$
4: update $l = l + 1$.
5: **until** the objective value keeps the same as the value obtained in the previous iteration

two blocks $\mathbf{A}$ and $\mathbf{Q}$ as defined in the beginning of this part. The user scheduling variables $\mathbf{A}$ and the UAV trajectory variables $\mathbf{Q}$ are then alternately optimized by solving P1.1 and P1.2′ correspondingly, while keeping the other block of variables fixed. In addition, the optimized variables in each iteration are served as inputs of the next iteration until there is no increase in objective value any more. For brevity, we summarize the iterative algorithm in Algorithm 4.

In the following, we prove the convergence of Algorithm 1. Define $\eta(\mathbf{A}_l, \mathbf{Q}_l)$ and $\eta^{\text{lb}}_{\text{trj}}(\mathbf{A}_l, \mathbf{Q}_l)$ as the objective value of P1 and P1.2′ respectively. It then follows that

$$\begin{aligned} \eta(\mathrm{A}_l, \mathbf{Q}_l) &\overset{a}{\leq} \eta(\mathrm{A}_{l+1}, \mathbf{Q}_l) \\ &\overset{b}{=} \eta^{\text{lb}}_{\text{trj}}(\mathrm{A}_{l+1}, \mathbf{Q}_l) \\ &\overset{c}{\leq} \eta^{\text{lb}}_{\text{trj}}(\mathrm{A}_{l+1}, \mathbf{Q}_{l+1}) \\ &\overset{d}{\leq} \eta(\mathrm{A}_{l+1}, \mathbf{Q}_{l+1}) \end{aligned} \tag{4.26}$$

where (a) holds since in step 2 of Algorithm 1, the optimal solution of P1.1 , which is $\mathbf{A}_{l+1}$, is obtained based on given $\mathbf{Q}_l$; (b) holds due to the fact that the first order Taylor expansions in (4.16) and (4.23) are tight at the given local location and the given local velocity respectively, so P1.2 and P1.2′ has the identical objective value; (c) holds since with the given $\mathbf{A}_{l+1}$ and $\mathbf{Q}_l$, P1.2′ is optimally solved in step 3 of Algorithm 1 with solution $\mathbf{Q}_{l+1}$; (d) holds as the objective value obtained by solving P1.2′ serves as the lower-bound of that of the original problem P1.2 at $\mathbf{Q}_{l+1}$.

Therefore, (4.26) suggests that the proposed algorithm is non-decreasing. Moreover, the objective value of P1 is clearly upper-bounded by a finite integer value, which corresponds to the total number of ground users. Therefore, the algorithm is guaranteed to converge.

4.3.2 Initial Trajectory Design

For successfully applying Algorithm 4, we need to feed an initial trajectory set $\mathbf{Q}$ into the system. It is known that both the convergence speed and performance of such iterative algorithm depend on the initialization schemes [77, 78]. In this subsection, we devise a simple initial trajectory for Algorithm 4 to achieve faster convergence and better user coverage performance.

In our specific scenario, the aerial BS has to return to the base for recharging at the end of the mission period, and a typical initial trajectory is circular trajectory [20, 53] which serves as the benchmark. Specifically, for the square geographical target area with side length L_s, we assume the center of the circular initial trajectory (CIT) is $\mathbf{c}_{\mathrm{t}} = [\frac{L_s}{2}, \frac{L_s}{2}]^T \in \mathbb{R}^{2\times 1}$. In addition, the radius of the circle is set as $r_{\mathrm{t}} = \frac{L_s}{4}$ so the number of users inside and outside the trajectory is balanced. We further assume that the base is located at $\mathbf{s}_{\mathrm{b}} = \mathbf{c}_{\mathrm{t}} + [r_{\mathrm{t}}, 0]^T = [\frac{L_s}{2} + r_{\mathrm{t}}, \frac{L_s}{2}]^T$.

Distinct from most of the UAV trajectory design problems, where the aerial BS associates with all the ground users, e.g. [20], only part of the ground users can be scheduled and associated in our specific problem. In this case, if CIT is fed to Algorithm 4, users which are closer to the initial trajectory has a higher opportunity to be considered for association due to the lower path loss. Additionally, users which are not scheduled in the first iteration will only be considered for association when the data request of all the scheduled users are met after optimizing the trajectory. In other words, CIT does not consider fair scheduling and association and may lead to a performance loss. This motivates us to devise a new initial trajectory which ensures all the ground users can get close to the UAV in certain time slots, so the users have a relatively fair opportunity to be scheduled. To this end, we design an initial trajectory where the UAV flies straightly from one ground user to the other with constant speed $\|\mathbf{v}[n]\| = V$ in the horizontal dimension, and finally backs to the

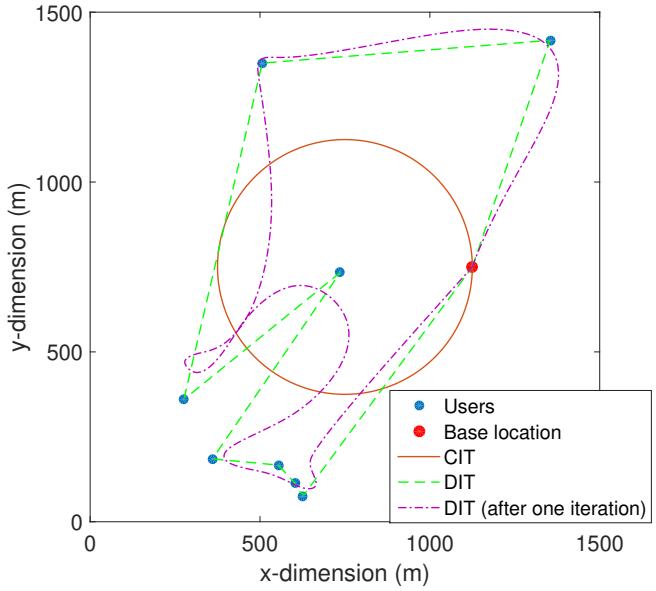

Figure 4.2: An example of CIT, DIT and the generated trajectory after one iteration of Algorithm 4 with DIT, $T = 100$s, $E_{\text{tot}} = 1.5 \times 10^4$J

base. The detailed procedure of the designed initial trajectory (DIT) is summarized as follows

1. Convert the location of ground users into polar coordinate system with $\mathbf{c}_{\text{t}}$ serves as the coordinate origin, that is $\mathbf{w}_i^{\text{p}} = [r_i, \theta_i]^T$, where $r_i = \|\mathbf{c}_{\text{t}} - \mathbf{w}_i\|$ and $\theta_i = \arctan(\frac{y_i - \frac{L_s}{2}}{x_i - \frac{L_s}{2}}) \in (0, 2\pi)$.

2. Starting from the base location, the designed path connects each of the ground users with a straight line based on a counterclockwise order. If two users have the same θ_i, the user which has a smaller r_i is prioritized.

3. Resort all the M users according to the access order in step 2, such that the first ground user is the one which has the smallest θ_i .

4. Calculate the total distance of DIT, which is

$$d_{\text{sum}} = \sum_{i=1}^{M-1} \|\mathbf{w}_{i+1} - \mathbf{w}_i\| + \|\mathbf{s}_{\text{b}} - \mathbf{w}_1\| + \|\mathbf{s}_{\text{b}} - \mathbf{w}_M\| \tag{4.27}$$

5. The distance interval is then calculated as $\delta_d = \frac{d_{\text{sum}}}{N}$, and the initial trajectory can be obtained accordingly.

Intuitively, the third step of Algorithm 4 forces the UAV to fly closer to the scheduled ground users in the corresponding time slots, so more data can be transmitted thanks to the decreased path loss. By applying DIT, the UAV-user distance is clearly reduced, and the proposed initial trajectory is also expected to speed up the convergence. However, note that the designed trajectory does not necessarily satisfy the UAV energy constraint (4.13f) and the mobility constraints (4.13k-4.13m). Fortunately, the third step of Algorithm 4 guarantees to generate a trajectory which satisfies all the above constraints, and the generated trajectory is based on a much fairer scheduling and association scheme compared to CIT. Therefore, the performance of Algorithm 4 is still non-decreasing and thus converges from the second iteration. For better illustration of the proposed initial trajectory, Fig. 4.2 compares CIT, DIT and the generated trajectory after one iteration of Algorithm 1 by applying DIT. Note that, the users which are located far away from CIT ,e.g., the one in the top right corner may never be scheduled and associated by applying CIT due to the large path loss. On the contrary, the data demand of these users might be satisfied by applying DIT thanks to the significantly reduced transmission distance.

4.4 Imperfect ULI and Robust Techniques

In real scenarios, the accuracy of GPS systems is affected by lots of factors such as weather and terrain [79]. Consequently, it is difficult to obtain accurate ULI in practice, and the number of served users may decrease drastically. In this section, we propose two robust techniques for compensating the performance loss in the existence of inaccurate ULI.

4.4.1 Worst Case (WC) ULI optimization

Firstly, we model the estimated user location as $\widetilde{\mathbf{w}}_i = [x_i + e_{xi}, y_i + e_{yi}]^T$, where e_{xi} and e_{yi} denote the estimation error in the x-axis and y-axis respectively. Both e_{xi} and e_{yi} follow Gaussian distribution with zero mean and standard deviation σ in meters. We assume that the maximum deviation between real user location and the estimated user location is d_{th}, where $d_{\text{th}} \approx 3\sigma$. It is clear that the real position of user i is bounded by a circle region with radius d_{th} and circle center $\widetilde{\mathbf{w}}_i$. For the aim of

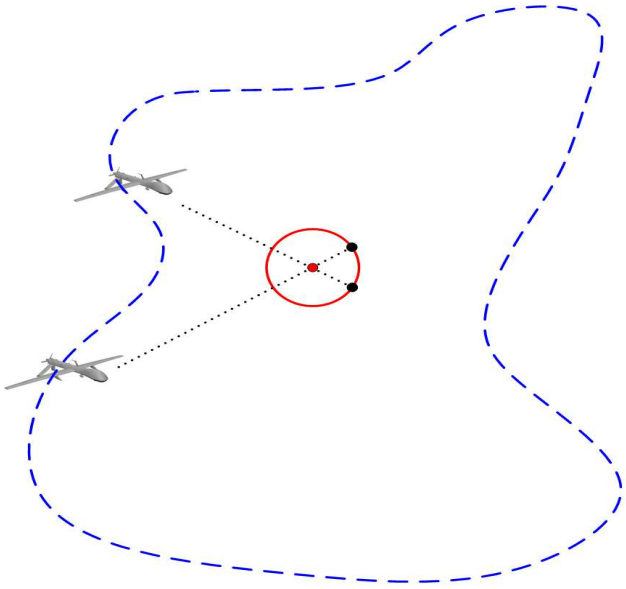

Figure 4.3: Optimizing the trajectory with respect to the worst case ULI

increasing the robustness against imperfect ULI, we first propose a simple technique which guarantees the coverage performance in the worst case. Instead of solving P1 with $\widetilde{\mathbf{w}}_i$, we employ the worst case ULI into Algorithm 4. The worst case user location at a specific time slot is the farthest intersection between the circle which specifies the region of actual user location and a straight line which starts from the UAV position $\mathbf{s}[n]$ and passes through $\widetilde{\mathbf{w}}_i$. As shown in Fig. 4.3, the estimated user location is represented by red dots. The worst case user location, on the other hand, is the farthest intersection point between the line and the red circle, and is represented by the black dot. Therefore, instead of solving P1, the proposed robust technique tries to find the optimal trajectory and optimal scheduling and association by solving the following problem

$$(\text{P2}): \quad \underset{\{\alpha_i[n],\mathbf{s}[n],\mathbf{v}[n],\mathbf{a}[n],\rho_i\}}{\text{Maximize}} \sum_{i\in M} \rho_i \tag{4.28a}$$

$$\text{subject to } (4.13\text{c}) - (4.13\text{m})$$

$$\sum_{n=1}^{N} \alpha_i[n] B \log_2(1+\widetilde{\gamma}_i[n]) \geq \rho_i Q_i, \forall i \tag{4.28b}$$

where we have

$$\widetilde{\gamma}_i[n]=\frac{P_t \cdot \zeta_0}{H^2+\left(\|\mathbf{s}[n]-\widetilde{\mathbf{w}}_i\|+d_{\text{th}}\right)^2} \tag{4.29}$$

As the LHS of (4.28b) is convex with respect to $\left(\|\mathbf{s}[n]-\widetilde{\mathbf{w}}_i\|+d_{\text{th}}\right)^2$ with given association variables, P2 can be solved by the same iterative algorithm as we used for solving P1. By solving P2, all the users that are covered in P2 are guaranteed to be covered in P1 with inaccurate ULI since the former considers the worst case performance.

4.4.2 Minimum Excess Data Maximization (MEDM)

In the preceding subsection, we increase the robustness by guaranteeing the worst case conditions. In this subsection, the robustness against inaccurate ULI is increased from another perspective. We first note that once the proposed iterative algorithm gives an optimal solution such that M_{s} users are covered, where $M_{\text{s}} \leq M$, N_{s} out of N time slots are allocated for satisfying the requirement of the M_{s} users. In other words, instead of providing more bits to the covered users, the aerial BS tries to allocate redundant time slots to meet the data demand of unsatisfied users. We assume $\mathscr{S}$ is a set which contains all the covered users. Therefore, for the m-th user in the set $\mathscr{S}$, we have $U_m \geq Q_m$. It is obvious that increased immunity to inaccurate ULI for the m-th covered user can be achieved by increasing the excessive data $\varepsilon_m = U_m - Q_m$, we thus propose a new robust technique by maximizing the minimum excessive data among covered users. The optimization problem associated with the robust technique is formulated as

$$\begin{aligned}
(\text{P3}): \quad & \underset{\{\alpha_m[n],\mathbf{s}[n],\mathbf{v}[n],\mathbf{a}[n]\}}{\text{Max min}} \left(U_m - Q_m\right) && \text{(4.30a)}\\
& \text{subject to } (4.13\text{f}) - (4.13\text{m}) \\
& \alpha_m[n] \in \{0,1\}, \forall n, \forall m && \text{(4.30b)}\\
& \sum_{m=1}^{M_{\text{s}}} \alpha_m[n] \leq 1, \forall n && \text{(4.30c)}
\end{aligned}$$

where

$$U_m = \sum_{n=1}^{N} \alpha_m[n] B \log_2(1+\gamma_m[n]) \tag{4.31}$$

$$\gamma_m[n] = \frac{P_t \cdot \zeta_0}{H^2 + \|\mathbf{s}[n] - \mathbf{w}_m\|^2}, m \in \mathscr{S} \tag{4.32}$$

In P3, all the time slots are allocated to the covered users, and the trajectory and association variables are optimized for increasing the minimum ε_m. The above optimization problem is equivalent to maximizing an auxiliary variable η, which represents the minimum excessive data as follows

$$\begin{aligned}
(\text{P3.1}): \quad & \max_{\{\alpha_m[n],\mathbf{s}[n],\mathbf{v}[n],\mathbf{a}[n],\eta\}} \eta && \text{(4.33a)}\\
& \text{subject to } (4.13\text{f}) - (4.13\text{m}) \\
& U_m - Q_m \geq \eta, \forall m && \text{(4.33b)}\\
& \alpha_m[n] \in \{0,1\}, \forall n, \forall m && \text{(4.33c)}\\
& \sum_{m=1}^{M_s} \alpha_m[n] \leq 1, \forall n && \text{(4.33d)}
\end{aligned}$$

The non-convex constraint (4.33b) in (P3.1) can be tackled with the same method as shown in (4.16)-(4.18), which yields

$$U_m^{\text{lb}} - Q_m \geq \eta, \forall m \tag{4.34}$$

Here, U_m^{lb} denotes the lower bound of U_m and is obtained by first order Taylor approximation.

$$\begin{aligned}
U_m^{\text{lb}} \triangleq & \sum_{n=1}^{N} \alpha_m[n] B \cdot B_m^l[n] \\
& - \sum_{n=1}^{N} \alpha_m[n] B \cdot A_m^l[n] \left(\|\mathbf{s}[n] - \mathbf{w}_m\|^2 - \|\mathbf{s}_l[n] - \mathbf{w}_m\|^2 \right)
\end{aligned} \tag{4.35}$$

where $A_m^l[n]$ and $B_m^l[n]$ are constants which are given by

$$A_m^l[n] = \frac{(\log_2 e) P_t \zeta_0}{(H^2 + \|\mathbf{s}_l[n] - \mathbf{w}_m\|^2)(H^2 + \|\mathbf{s}_l[n] - \mathbf{w}_m\|^2 + P_t \zeta_0)} \tag{4.36}$$

Table 4.1: Simulation parameters2

parameter	value	parameter	value
B	10^6 Hz	H	100 m
P_t	0.01 W	g	9.8 m/s^2
β_0	-50 dB	δ_t	0.5 s
σ^2	-110 dBm	$v_{\max}$	80 m/s
c_1	9.26×10^{-4}	$v_{\min}$	3 m/s
c_2	2250	$a_{\max}$	6 m/s^2

$$B_m^l[n] = \log_2(1 + \frac{P_t \zeta_0}{H^2 + \|\mathbf{s}_l[n] - \mathbf{w}_m\|^2}), \forall n, \forall m \tag{4.37}$$

Except the objective function and constraint (4.33b), the only difference between problem P3.1 and P1 is that the time slots in P3.1 can only be allocated to the covered users. The other two non-convex constraints in P3.1, which are (4.13f) and (4.13l) have already been addressed in (4.20)-(4.24). Therefore, P3.1 can be solved with the same iterative algorithm as shown in Algorithm 4. The difference is that, now the iterative algorithm is required to repeat until the fractional increase of the objective value is below a certain threshold $\varepsilon > 0$. With this robust method, all the covered users receive more bits than required. Therefore, even less bits are provided by the aerial BS due to the effect of inaccurate ULI, the corresponding users are still covered as long as $\widetilde{U_m} \geq Q_m, \forall m$, where $\widetilde{U_m}$ represents the actual total provided data to the m-th user.

4.5 Simulation Results

In this section, numerical results are provided to evaluate the performance of our proposed techniques. We assume $M = 8$ users are distributed randomly within the square target area of 1.5×1.5km^2. Correspondingly, the charging base is located at $[1125, 750]^T$ and the radius of CIT is $r_{\mathrm{t}} = 375$m. Unless otherwise stated, we use the parameters shown in Table 4.1. Moreover, we assume the data demand of each user is randomly chosen from the range of $[1, 20]$ Mbits. The coverage performance is evaluated with regard to user coverage probability, which is defined as the ratio of number of users with satisfied data demand to the total number of ground users within the target area. It is clear that, increased coverage probability can be obtained

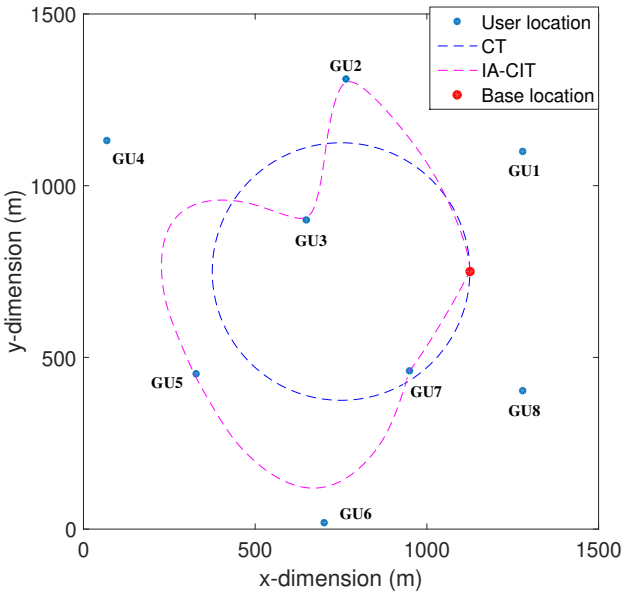

Figure 4.4: Optimized trajectory with IA-CIT, T=100 s, $E_{\text{tot}} = 1.5 \times 10^4$ J

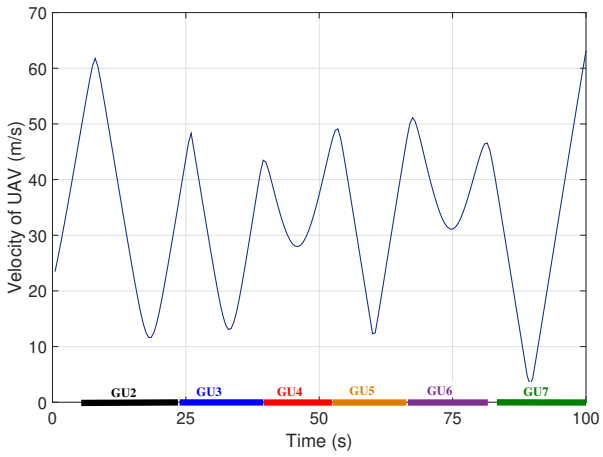

Figure 4.5: Speed of aerial BS corresponding to the trajectory shown in Fig. 4.4

by meeting the data demand of more ground users. For ease of presentation, the proposed iterative algorithm with CIT and DIT are termed as IA-CIT and IA-DIT respectively. Furthermore, the proposed robust technique which guarantees the worst case performance and the one which maximizes the minimum excessive data are namely WC and MEDM correspondingly.

4.5.1 Proposed Iterative Algorithm and the Impact of Time and Energy Constraints

In Fig. 4.4, we first illustrate the optimized trajectory obtained by the proposed IA-CIT, assuming T=100 s and $E_{\text{tot}} = 1.5 \times 10^4$ J. It can be observed that the UAV tries to move close to the associated users to reduce path loss and thus transmits more data. Although the ground users have different data demand, the users which are located closer to the initial trajectory have a better chance to be scheduled and associated thanks to the better communication condition. UAV acceleration constraint forbids the UAV to change its direction abruptly. This results in a smooth flight trajectory as can be seen in the figure. For better understanding the UAV's flying status, Fig. 4.5 shows the time-varying UAV speed and the user association status corresponding to the trajectory shown in Fig. 4.4. It can be seen that the UAV first flies towards the served users with increased speed, then gradually reduces its speed when it starts to have a good communication condition. Note that the fixed-wing UAV can not stay stationary above the associated users and this explains why the aerial BS always move with a positive speed. It can also be observed that not all the time slots are allocated for the covered users. This verifies that the aerial BS tries to allocate redundant time slots to users which can not be fully satisfied after meeting the requirement of the covered users.

The number of covered users is limited by both the mission period T and on-board energy resources E_{tot}. Firstly, Fig. 4.6 illustrates the optimized trajectories obtained by IA-CIT under different T with large enough on-board energy $E_{\text{tot}} = 2.5 \times 10^4$J. As can be seen in the figure, request of more ground users are satisfied with a longer time period, since more time slots are allocated for transmitting data. Ideally, it is expected that all the ground users can be covered when T is large enough. However, increasing T not only increases the user access delay but also increases the consumed energy. As T increases, each user needs to wait for a longer time to be associated and more built-in energy is consumed. Therefore, in real scenarios, the choice of T should consider both energy consumption and time-delay tradeoff.

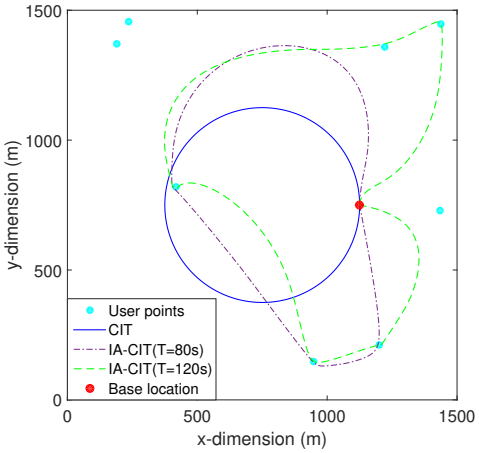

Figure 4.6: Optimized trajectory with IA-CIT for different time period T, $E_{\text{tot}} = 2.5 \times 10^4$ J

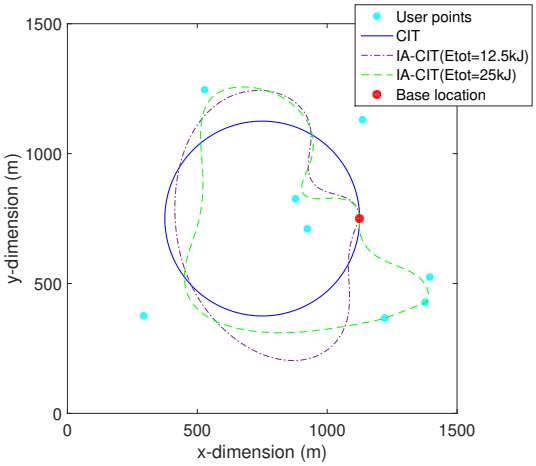

Figure 4.7: Optimized trajectory with IA-CIT for different on-board energy E_{tot}, T=120 s

On the contrary, Fig. 4.7 shows the optimized trajectories obtained by IA-CIT with various built-in energy resources under a large enough time period T=120 s. As expected, more users can be covered by increasing the total amount of on-board energy. On one hand, as E_{tot} increases, the aerial BS is able to move closer to the users which have been satisfied to enjoy a better communication condition. In this case, the covered users remain covered with a decreased association time and the redundant time slots can be allocated for other users which have not been satisfied yet. On the other hand, the aerial BS is able to move a longer distance to reach the users which are far away from the initial trajectory with increased E_{tot}.

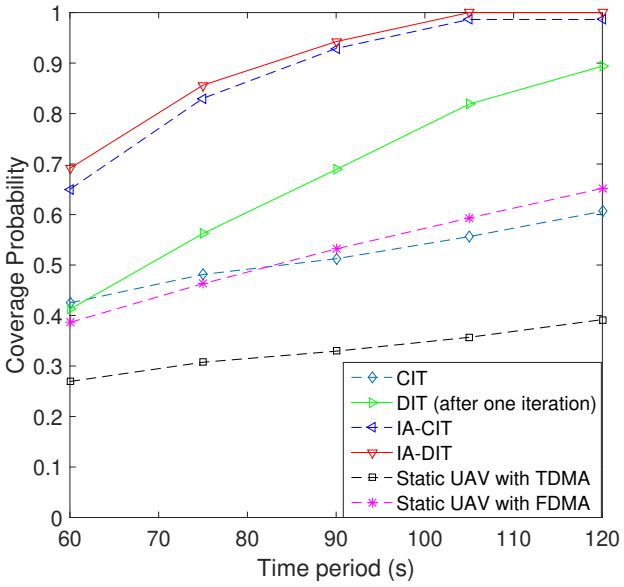

Figure 4.8: Coverage probability versus time period T with different techniques, $E_{\text{tot}} = 2.5 \times 10^4$J

4.5.2 Designed initial trajectory (DIT)

In this subsection, we evaluate the benefits of the proposed DIT. By assuming enough on-board energy $E_{\text{tot}} = 2.5 \times 10^4$J, Fig. 4.8 compares the achieved coverage probability for six different schemes, i.e., 1) CIT, which corresponds to a scheme using circular trajectory centered at $\mathbf{c}_{\text{t}} = [750, 750]^T$ with optimized scheduling and association variables; 2) DIT, which uses a fixed designed trajectory and optimized scheduling and association variables. Note that DIT actually represents the trajectory generated after one iteration of Algorithm 4 and thus meets the velocity and acceleration constraints; 3) IA-CIT; 4)IA-DIT; 5) Static UAV with TDMA, where the aerial BS is placed at a fixed location above $\mathbf{c}_{\text{t}}$ with altitude equals 100 meters. In addition, the static aerial BS communicates with ground users by TDMA scheme, which is the same as the case of moving aerial BS, so the scheduling and association variables are optimized; 6) Static UAV with FDMA, where the same static aerial BS as in 5) is utilized, but we change the access method to FDMA. In other word, each user is associated for the entire T but with a reduced a bandwidth $B_i = \frac{B}{M} = 1.25 \times 10^5$ Hz.

As regards the performance observed, we can first conclude that, a signifi-

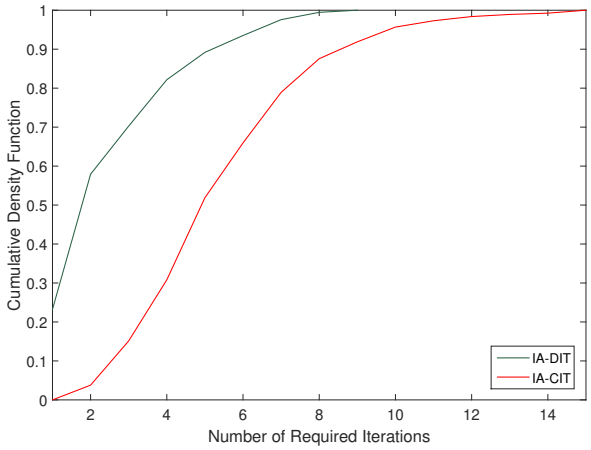

Figure 4.9: CDF of number of required iterations for IA-CIT and IA-DIT, $E_{\text{tot}} = 2.5 \times 10^4$J, T=120 s

cantly increased coverage performance can be achieved by exploiting the mobility of UAV due to the reduced communication distance, thus reduced path loss. Moving aerial BSs achieve at least 20% higher coverage probability than static aerial BS using TDMA. Fig. 4.8 also shows that static aerial BS covers more users by applying FDMA. However, the technique still covers at least 25% less users than the techniques exploiting the mobility of UAV except CIT when T=120 s. As expected, DIT satisfies the data demand of more ground users than CIT, and the performance gap between DIT and CIT becomes larger as T increases. This is because with a longer mission period, DIT is able to move even closer to each of the users and enjoys a better communication channel compared to CIT. Finally, it can be observed that the use of DIT further increases the coverage probability of the proposed iterative algorithm. It is worth mentioning that, IA-CIT can not cover 100 % ground users even with large enough T. IA-DIT, on the other hand, is able to fill the performance gap and cover all the ground users as long as longer enough T and large enough E_{tot} is given.

Fig. 4.9 verifies that the devised initial trajectory can speed up the convergence. It can be seen that IA-CIT requires at most 15 iterations to converge while IA-DIT is guaranteed to converge within 9 iterations. This is as expected since the trajectory optimization forces the UAV to move closer to the associated users, and

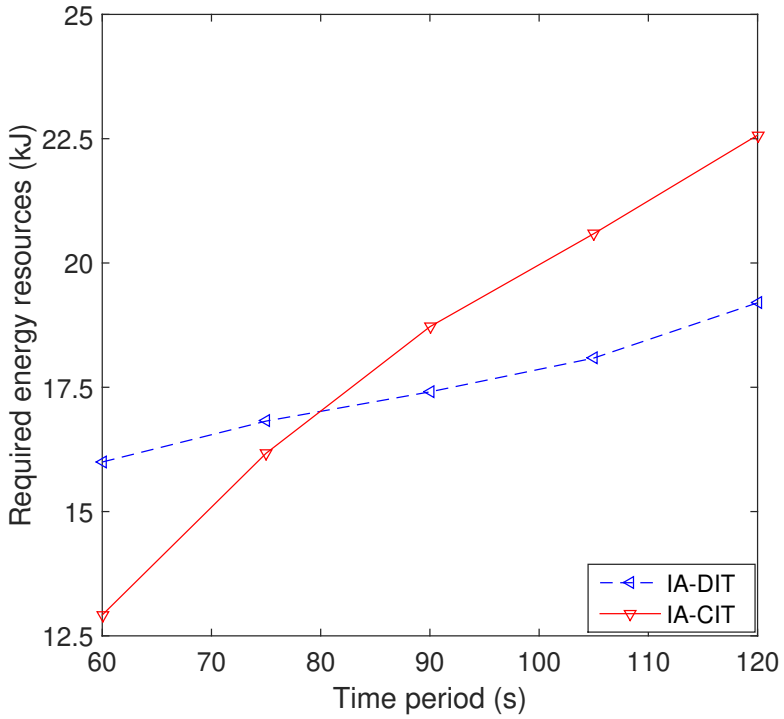

Figure 4.10: Average energy consumption for IA-CIT and IA-DIT, $E_{\text{tot}} = 2.5 \times 10^4$J

DIT provides a reduced distance with the covered users compared to CIT.

Fig. 4.10 further compares the average energy consumption for IA-CIT and IA-DIT, with $E_{\text{tot}} = 2.5 \times 10^4$J. It can be seen that more energy are consumed by IA-DIT when we have a short time period. This is because with a small number of time slots for association, IA-DIT requires the aerial BS to move faster and change its directions more abruptly compared to IA-CIT. However, the energy consumption of IA-CIT increases more drastically than IA-DIT as T increases. Specifically, the average consumed energy of IA-CIT exceeds IA-DIT when T=80s, and IA-CIT consumes approximately 3.5×10^3 more energy when T=120s.

4.5.3 ULI-robust techniques

In practice, it is difficult to estimate ULI accurately. Therefore, it is meaningful to examine the coverage performance of the proposed IA-CIT and IA-DIT techniques in the existence of inaccurate ULI. We assume $E_{\text{tot}} = 2.5 \times 10^4$J and T=100 s, and the corresponding results are shown in Fig. 4.11. It can be observed that the performance of both IA-CIT and IA-DIT decreases significantly when introducing

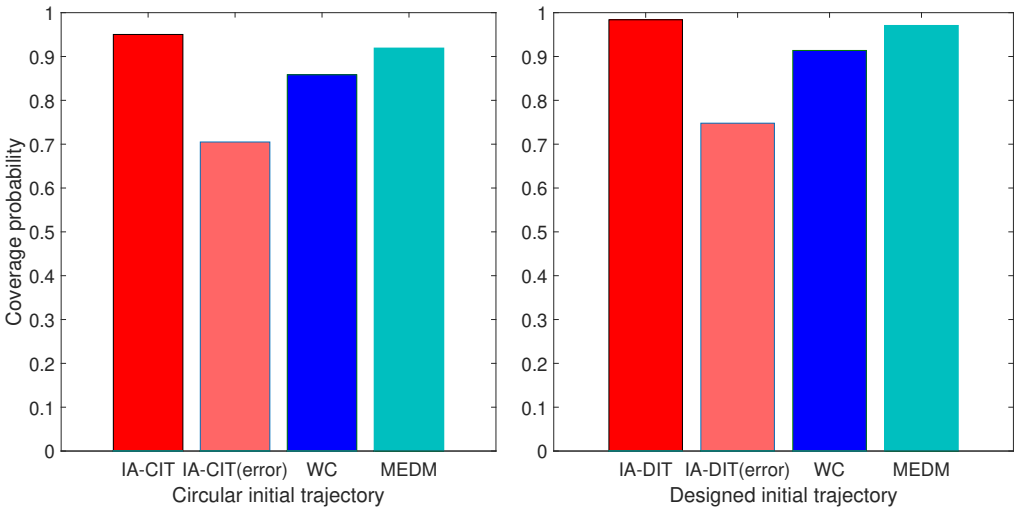

Figure 4.11: Coverage probability with imperfect ULI and Robust techniques, $E_{\text{tot}} = 2.5 \times 10^4$J, T=100 s

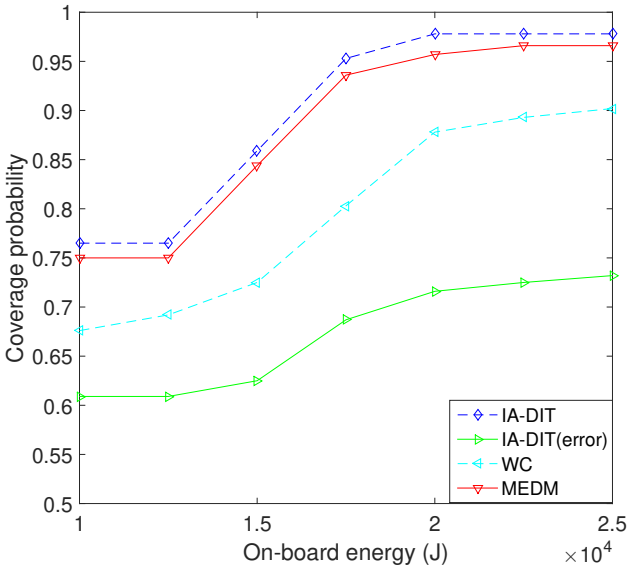

Figure 4.12: Coverage performance of Robust techniques versus various on-board energy E_{tot}, T=100 s

inaccurate ULI. For example, IA-DIT covers approximately 98% of total users with accurate ULI. However, the coverage probability decreases by 25% when inaccurate ULI is applied, as a result of more severe path loss than expected. Note that the performance loss is greatly compensated with the proposed robust techniques as shown in Figure. 4.11. WC technique guarantees the worst case performance and thus increases the immunity to imperfect ULI. MEDM technique, on the other

hand, provides excessive data to each of the covered users and achieves even better coverage probability than WC. When DIT is used, the decreased coverage performance in the existence of imperfect ULI is almost completely compensated by applying MEDM.

Fig. 4.12 further shows the coverage performance of the proposed robust techniques versus various on-board energy resources. First note that the achieved coverage probability of IA-DIT increases as more on-board energy is available, which is consistent with the result shown in Fig. 4.7. In the meanwhile, the coverage performance decreases by more than 20 % after introducing imperfect ULI. With increased on-board energy, the UAV is able to move closer to the worst case user locations to reduce path loss, so WC technique is able to satisfy the data demand of more ground users. Similarly, more performance loss can be compensated by MEDM thanks to increased on-board energy, since more excessive data can be provided to the satisfied users. Notably, with the change of E_{tot}, an approximately 7% coverage performance gap remains between WC and MEDM.

4.6 Summary

In this chapter, we study the bottom lie aim of aerial BS application, where an aerial BS is dispatched for satisfying the data demand of a maximum number of ground users before exhausting its on-board energy. An iterative algorithm based on successive convex optimization and alternating optimization techniques is proposed. The iterative algorithm alternately optimizes the UAV trajectory and user scheduling and association in each iteration. In order to speed up the convergence and further improve the coverage performance, we devise an initial trajectory such that all the ground users have a relatively fair chance to be scheduled and associated. Moreover, the existence of imperfect ULI is considered and two different robust techniques, one aiming at guaranteeing the worst case performance, the other maximizing the minimum excess data to the covered users are proposed correspondingly.

Chapter 5

Conclusions and Future Work

5.1 Conclusions

For satisfying the incessantly increasing and highly diversified data demand, it is envisioned that UAVs will become an indispensable part in the future communication systems. In this thesis, we focus on UAVs serving as aerial BSs to provide wireless services to ground users from the sky.

We firstly summarized the main advantages and potential use cases of UAVs. UAVs which are flexible and cost-effective have a wide range of applications including assisting D2D networks, serving as enabler for mmWave techniques, collecting and disseminating data in IoT networks, Relaying, enabling WPT in special scenarios and most importantly, serving as aerial BSs to provide fast and reliable communication services. After concluding the potential applications, we further summarized the main research directions and challenges of UAV-based aerial BSs.

The efficient deployment of multiple static aerial BSs was considered. With the proposed successive deployment method based on geometrical relaxation, we enabled the simultaneous use of multiple aerial BSs while avoiding ICI. For reducing the computational complexity, we further proposed two simultaneous deployment methods with the help of K-means clustering. The simultaneous deployment techniques are especially useful when ground users are distributed unevenly. While SD-KM and SD-KMVR not only achieve better coverage performance but also save power and costs, the SD-GR method finds its unique use when only a small number

of aerial BSs is available. We found that there is a tradeoff between power efficiency and immunity to inaccurate ULI. Increased robustness can be achieved with larger coverage area, which however also incurs larger transmit power.

We then fully exploited the mobility of UAVs. By applying an efficient iterative algorithm to optimize both the UAV trajectory and UAV-user scheduling and association, we satisfied the data demand of a maximum number of ground users without exhausting the limited on-board energy of a moving aerial BS. It was shown that the aerial BS increases its flying speed when it has a large distance between the served ground user, and slows down when it starts to have a good communication condition with small path loss. Furthermore, by devising an initial trajectory which considers the fairness, we speed up the convergence of the iterative algorithm and improve the coverage performance. The existence of imperfect ULI was again considered. It was shown that increased robustness can be achieved by either guaranteeing the worst case performance or providing excess data bits to covered users.

5.2 Future Work

The proposed techniques in this thesis have motivated further investigations in some research directions. Specifically, the following research lines are of interest to the author for future work:

- Regarding both the deployment of static aerial BSs and the trajectory design of moving aerial BSs, it will be interesting to investigate adaptive deployment scheme, where the aerial BS adapts its location to serve moving users with instantaneous traffic. Our work assumes that the user points are placed at fixed locations, which is relevant in some specific scenarios, but also limits its use. In practice, the location of users various with time. The dynamic movement of UAVs can be captured by random waypoint (RWP) model. By applying such model, each user randomly chooses a destination point in the area and moves with constant speed on a straight line to this point. After waiting a random pause time, the user chooses a new destination point and speed, and so on. In addition, the data demand of users changes with time as well. In this case,

the techniques proposed for the low-mobility and delay-tolerant ground users cannot cater well to the real-time demands of mobile users. It is expected that, compared to ground BSs, we may achieve a significant performance gain if we adaptively change the location of aerial BSs, letting UAVs chase the users.

- As introduced in this thesis, most UAVs are powered by limited on-board batteries, which greatly affect the performance and endurance of aerial BSs. When on-board battery is used, we need to prepare few backup aerial BSs, and the dispatched UAV should frequently fly back to the base for recharging. Therefore, it is interesting to study solar-powered UAVs which enables sustainable aerial BSs. In addition, with the use of solar-powered UAVs, we have a surge of new challenges to overcome. For example, more solar power can be harvested when UAV is deployed at a higher altitude. However, higher altitude also leads to increased AtG communication path loss. Therefore, there is an intrinsic communication performance-endurance tradeoff to study.

- The third research line is the collective use of UAV and Radar system. Equipped with Radar systems, aerial BSs can realize communication and radar functions at the same time, which greatly reduces the cost. Additionally, the shared use of hardware between transceivers and sensors reduced the required payload of UAV, thus further increases the endurance of aerial BSs.

- The other research line may consider the joint use of multiple static aerial BSs and moving aerial BSs. Note that the proposed SD-GR, SD-KM and SD-KMVR techniques cannot guarantee a 100% coverage, leaving the users located in the in-between areas uncovered. The data requirement of these uncovered users might be satisfied by deploying the moving aerial BS which operates at a separate frequency band. Alternatively, D2D connections, which allow direct transmission between two nearby users, may also be studied in future to accommodate the uncovered users. In such scenario, aerial BSs and D2D connections are jointly leveraged to provide wireless service for more users. In fact, instead of just maximizing the coverage probability, more inter-

esting problems can be studied under such background. For instance, we may want to maximize the system sum rate, where new problems arise. The user association, for example, can be quite complex since we want to determine whether a user is associated with either a particular aerial BS or a particular UAV-served user, or should remain isolated to save wireless resource for other users with better communication conditions.

Bibliography

[1] O. Semiari, W. Saad, M. Bennis, and Z. Dawy. Inter-Operator Resource Management for Millimeter Wave Multi-Hop Backhaul Networks. *IEEE Transactions on Wireless Communications*, 16(8):5258–5272, Aug 2017.

[2] A. Li and C. Masouros. Hybrid Analog-Digital Millimeter-Wave MU-MIMO Transmission With Virtual Path Selection. *IEEE Communications Letters*, 21(2):438–441, Feb 2017.

[3] Y. Zhang, L. Song, W. Saad, Z. Dawy, and Z. Han. Contract-Based Incentive Mechanisms for Device-to-Device Communications in Cellular Networks. *IEEE Journal on Selected Areas in Communications*, 33(10):2144–2155, Oct 2015.

[4] W. Song, Y. Zhao, and W. Zhuang. Stable Device Pairing for Collaborative Data Dissemination With Device-to-Device Communications. *IEEE Internet of Things Journal*, 5(2):1251–1264, April 2018.

[5] M. Dessouky, M. Nofal, H. Sharshar, and Y. Albagory. Optimization of Beams Directions for High Altitude Platforms Cellular Communications Design. In *Proceedings of the Twenty Third National Radio Science Conference (NRSC'2006)*, pages 1–8, March 2006.

[6] D. A. J. Pearce and D. Grace. Optimum Antenna Configurations for Millimetre-wave Communications from High-altitude Platforms. *IET Communications*, 1(3):359–364, June 2007.

[7] T. Celcer, T. Javornik, M. Mohorcic, and G. Kandus. Virtual multiple input multiple output in multiple high-altitude platform constellations. *IET Communications*, 3(11):1704–1715, November 2009.

[8] Mohammad Mozaffari, Walid Saad, Mehdi Bennis, Young-Han Nam, and Mérouane Debbah. A Tutorial on UAVs for Wireless Networks: Applications, Challenges, and Open Problems. *CoRR*, abs/1803.00680, 2018.

[9] A. Asadi, Q. Wang, and V. Mancuso. A Survey on Device-to-Device Communication in Cellular Networks. *IEEE Communications Surveys Tutorials*, 16(4):1801–1819, Fourthquarter 2014.

[10] M. N. Tehrani, M. Uysal, and H. Yanikomeroglu. Device-to-device communication in 5G cellular networks: challenges, solutions, and future directions. *IEEE Communications Magazine*, 52(5):86–92, May 2014.

[11] Y. Zeng, R. Zhang, and T. J. Lim. Wireless Communications with Unmanned Aerial Vehicles: Opportunities and Challenges. *IEEE Communications Magazine*, 54(5):36–42, May 2016.

[12] A. Orsino, A. Ometov, G. Fodor, D. Moltchanov, L. Militano, S. Andreev, O. N. C. Yilmaz, T. Tirronen, J. Torsner, G. Araniti, A. Iera, M. Dohler, and Y. Koucheryavy. Effects of Heterogeneous Mobility on D2D- and Drone-Assisted Mission-Critical MTC in 5G. *IEEE Communications Magazine*, 55(2):79–87, February 2017.

[13] Mohammad Mozaffari, Walid Saad, Mehdi Bennis, Young-Han Nam, and Mérouane Debbah. A Tutorial on UAVs for Wireless Networks: Applications, Challenges, and Open Problems. *CoRR*, abs/1803.00680, 2018.

[14] Z. Pi and F. Khan. An Introduction to Millimeter-wave Mobile Broadband Systems. *IEEE Communications Magazine*, 49(6):101–107, June 2011.

[15] M. Gapeyenko, V. Petrov, D. Moltchanov, S. Andreev, N. Himayat, and Y. Koucheryavy. Flexible and Reliable UAV-Assisted Backhaul Operation in

5G mmWave Cellular Networks. *IEEE Journal on Selected Areas in Communications*, 36(11):2486–2496, Nov 2018.

[16] I. Bor-Yaliniz and H. Yanikomeroglu. The New Frontier in RAN Heterogeneity: Multi-Tier Drone-Cells. *IEEE Communications Magazine*, 54(11):48–55, November 2016.

[17] N. Rupasinghe, Y. Yapici, I. Gven, and Y. Kakishima. Non-orthogonal multiple access for mmWave drones with multi-antenna transmission. In *2017 51st Asilomar Conference on Signals, Systems, and Computers*, pages 958–963, Oct 2017.

[18] J. Zhao, F. Gao, L. Kuang, Q. Wu, and W. Jia. Channel Tracking With Flight Control System for UAV mmWave MIMO Communications. *IEEE Communications Letters*, 22(6):1224–1227, June 2018.

[19] C. Zhan, Y. Zeng, and R. Zhang. Energy-Efficient Data Collection in UAV Enabled Wireless Sensor Network. *IEEE Wireless Communications Letters*, 7(3):328–331, June 2018.

[20] Q. Wu, Y. Zeng, and R. Zhang. Joint Trajectory and Communication Design for Multi-UAV Enabled Wireless Networks. *IEEE Transactions on Wireless Communications*, 17(3):2109–2121, March 2018.

[21] Z. Dawy, W. Saad, A. Ghosh, J. G. Andrews, and E. Yaacoub. Toward Massive Machine Type Cellular Communications. *IEEE Wireless Communications*, 24(1):120–128, February 2017.

[22] M. Mozaffari, W. Saad, M. Bennis, and M. Debbah. Mobile Unmanned Aerial Vehicles (UAVs) for Energy-Efficient Internet of Things Communications. *IEEE Transactions on Wireless Communications*, 16(11):7574–7589, Nov 2017.

[23] B. Pearre and T. X. Brown. Model-free Trajectory Optimization for Wireless Data Ferries among Multiple Sources. In *2010 IEEE Globecom Workshops*, pages 1793–1798, Dec 2010.

[24] Y. Zeng and R. Zhang. Energy-Efficient UAV Communication With Trajectory Optimization. *IEEE Transactions on Wireless Communications*, 16(6):3747–3760, June 2017.

[25] S. Samarakoon, M. Bennis, W. Saad, M. Debbah, and M. Latva-aho. Ultra Dense Small Cell Networks: Turning Density Into Energy Efficiency. *IEEE Journal on Selected Areas in Communications*, 34(5):1267–1280, May 2016.

[26] A. Al-Hourani, S. Kandeepan, and S. Lardner. Optimal LAP Altitude for Maximum Coverage. *IEEE Wireless Communications Letters*, 3(6):569–572, Dec 2014.

[27] R. I. Bor-Yaliniz, A. El-Keyi, and H. Yanikomeroglu. Efficient 3-D Placement of an Aerial Base Station in Next Generation Cellular Networks. In *2016 IEEE International Conference on Communications (ICC)*, pages 1–5, May 2016.

[28] E. Kalantari, M. Z. Shakir, H. Yanikomeroglu, and A. Yongacoglu. Backhaul-aware Robust 3D Drone Placement in 5G+ Wireless Networks. In *2017 IEEE International Conference on Communications Workshops (ICC Workshops)*, pages 109–114, May 2017.

[29] E. Kalantari, I. Bor-Yaliniz, A. Yongacoglu, and H. Yanikomeroglu. User Association and Bandwidth Allocation for Terrestrial and Aerial Base Stations with Backhaul Considerations. In *2017 IEEE 28th Annual International Symposium on Personal, Indoor, and Mobile Radio Communications (PIMRC)*, pages 1–6, Oct 2017.

[30] B. Galkin, J. Kibilda, and L. A. DaSilva. Deployment of UAV-mounted Access Points According to Spatial User Locations in Two-tier Cellular Networks. In *2016 Wireless Days (WD)*, pages 1–6, March 2016.

[31] S. Zhang, H. Zhang, Q. He, K. Bian, and L. Song. Joint Trajectory and Power Optimization for UAV Relay Networks. *IEEE Communications Letters*, 22(1):161–164, Jan 2018.

[32] C. M. Cheng et al. Maximizing Throughput of UAV-Relaying Networks with the Load-Carry-and-Deliver Paradigm. In *2007 IEEE Wireless Communications and Networking Conference*, pages 4417–4424, March 2007.

[33] D. H. Choi, S. H. Kim, and D. K. Sung. Energy-efficient Maneuvering and Communication of a Single UAV-based Relay. *IEEE Transactions on Aerospace and Electronic Systems*, 50(3):2320–2327, July 2014.

[34] P. Zhan, K. Yu, and A. L. Swindlehurst. Wireless Relay Communications with Unmanned Aerial Vehicles: Performance and Optimization. *IEEE Transactions on Aerospace and Electronic Systems*, 47(3):2068–2085, July 2011.

[35] A. Merwaday and I. Guvenc. UAV Assisted Heterogeneous Networks for Public Safety Communications. In *2015 IEEE Wireless Communications and Networking Conference Workshops (WCNCW)*, pages 329–334, March 2015.

[36] W. Khawaja, O. Ozdemir, and I. Guvenc. UAV Air-to-Ground Channel Characterization for mmWave Systems. In *2017 IEEE 86th Vehicular Technology Conference (VTC-Fall)*, pages 1–5, Sep. 2017.

[37] M. Alzenad et al. 3-D Placement of an Unmanned Aerial Vehicle Base Station for Maximum Coverage of Users With Different QoS Requirements. *IEEE Wireless Communications Letters*, 7(1):38–41, Feb 2018.

[38] J. Sun and C. Masouros. Deployment Strategies of Multiple Aerial BSs for User Coverage and Power Efficiency Maximization. *IEEE Transactions on Communications*, pages 1–1, 2018.

[39] G. Yang, C. K. Ho, R. Zhang, and Y. L. Guan. Throughput Optimization for Massive MIMO Systems Powered by Wireless Energy Transfer. *IEEE Journal on Selected Areas in Communications*, 33(8):1640–1650, Aug 2015.

[40] J. Xu, Y. Zeng, and R. Zhang. UAV-Enabled Wireless Power Transfer: Trajectory Design and Energy Optimization. *IEEE Transactions on Wireless Communications*, 17(8):5092–5106, Aug 2018.

[41] Z. Yun and M. F. Iskander. Ray Tracing for Radio Propagation Modeling: Principles and Applications. *IEEE Access*, 3:1089–1100, 2015.

[42] M. M. Azari, F. Rosas, K. Chen, and S. Pollin. Ultra Reliable UAV Communication Using Altitude and Cooperation Diversity. *IEEE Transactions on Communications*, 66(1):330–344, Jan 2018.

[43] Alenka Zajic. *Mobile-to-Mobile Wireless Channels*. Artech House, Inc., Norwood, MA, USA, 2013.

[44] J. Holis and P. Pechac. Elevation Dependent Shadowing Model for Mobile Communications via High Altitude Platforms in Built-Up Areas. *IEEE Transactions on Antennas and Propagation*, 56(4):1078–1084, April 2008.

[45] M. Mozaffari, W. Saad, M. Bennis, and M. Debbah. Drone Small Cells in the Clouds: Design, Deployment and Performance Analysis. In *2015 IEEE Global Communications Conference (GLOBECOM)*, pages 1–6, Dec 2015.

[46] M. M. Azari, Y. Murillo, O. Amin, F. Rosas, M. Alouini, and S. Pollin. Coverage Maximization for a Poisson Field of Drone Cells. In *2017 IEEE 28th Annual International Symposium on Personal, Indoor, and Mobile Radio Communications (PIMRC)*, pages 1–6, Oct 2017.

[47] M. Alzenad, A. El-Keyi, F. Lagum, and H. Yanikomeroglu. 3-D Placement of an Unmanned Aerial Vehicle Base Station (UAV-BS) for Energy-Efficient Maximal Coverage. *IEEE Wireless Communications Letters*, 6(4):434–437, Aug 2017.

[48] M. Mozaffari, W. Saad, M. Bennis, and M. Debbah. Efficient Deployment of Multiple Unmanned Aerial Vehicles for Optimal Wireless Coverage. *IEEE Communications Letters*, 20(8):1647–1650, Aug 2016.

[49] J. Lyu, Y. Zeng, R. Zhang, and T. J. Lim. Placement Optimization of UAV-Mounted Mobile Base Stations. *IEEE Communications Letters*, 21(3):604–607, March 2017.

[50] A. Rucco, A. P. Aguiar, and J. Hauser. Trajectory optimization for constrained UAVs: A Virtual Target Vehicle approach. In *2015 International Conference on Unmanned Aircraft Systems (ICUAS)*, pages 236–245, June 2015.

[51] J. Lyu, Y. Zeng, and R. Zhang. Cyclical Multiple Access in UAV-Aided Communications: A Throughput-Delay Tradeoff. *IEEE Wireless Communications Letters*, 5(6):600–603, Dec 2016.

[52] Q. Wu and R. Zhang. Delay-constrained throughput maximization in UAV-enabled OFDM systems. In *2017 23rd Asia-Pacific Conference on Communications (APCC)*, pages 1–6, Dec 2017.

[53] J. Lyu, Y. Zeng, and R. Zhang. UAV-Aided Offloading for Cellular Hotspot. *IEEE Transactions on Wireless Communications*, 17(6):3988–4001, June 2018.

[54] K. Dogancay. UAV Path Planning for Passive Emitter Localization. *IEEE Transactions on Aerospace and Electronic Systems*, 48(2):1150–1166, APRIL 2012.

[55] F. Jiang and A. L. Swindlehurst. Optimization of UAV Heading for the Ground-to-Air Uplink. *IEEE Journal on Selected Areas in Communications*, 30(5):993–1005, June 2012.

[56] J. Xu, Y. Zeng, and R. Zhang. UAV-enabled Multiuser Wireless Power Transfer: Trajectory Design and Energy Optimization. In *2017 23rd Asia-Pacific Conference on Communications (APCC)*, pages 1–6, Dec 2017.

[57] D. Yang, Q. Wu, Y. Zeng, and R. Zhang. Energy Trade-off in Ground-to-UAV Communication via Trajectory Design. *IEEE Transactions on Vehicular Technology*, pages 1–1, 2018.

[58] J. Lu, S. Wan, X. Chen, and P. Fan. Energy-Efficient 3D UAV-BS Placement versus Mobile Users' Density and Circuit Power. In *2017 IEEE Globecom Workshops (GC Wkshps)*, pages 1–6, Dec 2017.

[59] L. Gupta, R. Jain, and G. Vaszkun. Survey of Important Issues in UAV Communication Networks. *IEEE Communications Surveys Tutorials*, 18(2):1123–1152, Secondquarter 2016.

[60] M. Mozaffari, W. Saad, M. Bennis, and M. Debbah. Optimal transport theory for power-efficient deployment of unmanned aerial vehicles. In *2016 IEEE International Conference on Communications (ICC)*, pages 1–6, May 2016.

[61] K. Li, W. Ni, X. Wang, R. P. Liu, S. S. Kanhere, and S. Jha. Energy-Efficient Cooperative Relaying for Unmanned Aerial Vehicles. *IEEE Transactions on Mobile Computing*, 15(6):1377–1386, June 2016.

[62] S. Kandeepan, K. Gomez, L. Reynaud, and T. Rasheed. Aerial-terrestrial Communications: Terrestrial Cooperation and Energy-efficient Transmissions to Aerial Base Stations. *IEEE Transactions on Aerospace and Electronic Systems*, 50(4):2715–2735, October 2014.

[63] M. Hua, Y. Wang, Z. Zhang, C. Li, Y. Huang, and L. Yang. Power-Efficient Communication in UAV-Aided Wireless Sensor Networks. *IEEE Communications Letters*, 22(6):1264–1267, 2018.

[64] David Tse and Pramod Viswanath. *Fundamentals of Wireless Communication*. Cambridge University Press, New York, NY, USA, 2005.

[65] Andrea Goldsmith. *Wireless Communications*. Cambridge University Press, New York, NY, USA, 2005.

[66] X. Xu, Y. Zeng, Y. L. Guan, and R. Zhang. Overcoming Endurance Issue: UAV-Enabled Communications With Proactive Caching. *IEEE Journal on Selected Areas in Communications*, 36(6):1231–1244, June 2018.

[67] Andreas Molisch. *Wireless Communications*. Wiley-IEEE Press, 2005.

[68] J. Illian, P.A. Penttinen, H. Stoyan, and D. Stoyan. *Statistical Analysis and Modelling of Spatial Point Patterns*. Statistics in Practice. Wiley, 2008.

[69] Adrian Baddeley. *Spatial Point Processes and their Applications*, volume 1892, pages 1–75. Springer, Netherlands, 2007.

[70] Qualcomm. LTE Unmanned Aircraft Systems-Trial Report. *Qualcomm Technologies*, February 2017.

[71] Z. q. Luo, W. k. Ma, A. M. c. So, Y. Ye, and S. Zhang. Semidefinite Relaxation of Quadratic Optimization Problems. *IEEE Signal Processing Magazine*, 27(3):20–34, May 2010.

[72] Rui Xu and Don Wunsch. *Clustering*. Wiley-IEEE Press, 2009.

[73] Stephen Boyd and Lieven Vandenberghe. *Convex Optimization*. Cambridge University Press, New York, NY, USA, 2004.

[74] F. Liu, C. Masouros, A. Li, H. Sun, and L. Hanzo. MU-MIMO Communications With MIMO Radar: From Co-Existence to Joint Transmission. *IEEE Transactions on Wireless Communications*, 17(4):2755–2770, April 2018.

[75] A. Li, C. Masouros, F. Liu, and A. L. Swindlehurst. Massive MIMO 1-Bit DAC Transmission: A Low-Complexity Symbol Scaling Approach. *IEEE Transactions on Wireless Communications*, 17(11):7559–7575, Nov 2018.

[76] Y. Zeng, R. Zhang, and T. J. Lim. Throughput Maximization for UAV-Enabled Mobile Relaying Systems. *IEEE Transactions on Communications*, 64(12):4983–4996, Dec 2016.

[77] M. Hong, M. Razaviyayn, Z. Luo, and J. Pang. A Unified Algorithmic Framework for Block-Structured Optimization Involving Big Data: With Applications in Machine Learning and Signal Processing. *IEEE Signal Processing Magazine*, 33(1):57–77, Jan 2016.

[78] J. Zhang, Y. Zeng, and R. Zhang. UAV-Enabled Radio Access Network: Multi-Mode Communication and Trajectory Design. *IEEE Transactions on Signal Processing*, 66(20):5269–5284, Oct 2018.

[79] Nyen Thin Li, Lau Ting, Nor Adila Husna, and Heikal Husin. GPS Systems Literature: Inaccuracy Factors And Effective Solutions. *International journal of Computer Networks & Communications*, 8:123–131, 04 2016.